Published in : Structures (2023), vol. 58, 105274
DOI: 10.1016/j.istruc.2023.105274
Status : Postprint (Author's version)

BUCKLING RESISTANCE OF STAR-BATTENED ANGLE MEMBERS MADE OF HIGH-STRENGTH STEEL

Marios-Zois Bezas [a,*], Sofia Antonodimitraki [a,b], Andre Beyer [c], Jeroen Van Wittenberghe [d], Muhammad-Omer Anwaar [e], Jan Maesschalck [f], Jean-Pierre Jaspart [a], Jean-François Demonceau [a]

[a]*Steel and Composite Construction, UEE Research Unit, Liège University, Belgium*

[b]*School of Civil Engineering, Institute of Steel Structures, National Technical University of Athens, Athens, Greece*

[c]*CTICM, Saint Aubin, France*

[d]*ArcelorMittal Global R&D Gent – OCAS NV, Belgium*

[e]*ArcelorMittal Global R&D, Luxembourg*

[f]*Elia Transmission Belgium SA/NV, Brussels, Belgium*

Keywords:

Buckling, star-battened section, built-up section, Angle profile, High-strength steel

Abstract

Recent upwards developments of the power grid requests lead to use of high strength steels (HSS) for the design and construction of higher and heavier loaded steel lattice transmission towers, or to strengthen the existing ones. Usually star-battened sections are preferred for the strengthening of individual members or in case of very high compression loads. Thus, the investigations focus here on the bearing capacity of a star-battened member made of two S460 L250x250x28 angles. The objective was to use a star-battened member made of two S460 L300x300x35 angles with a member length of 4486 mm that will be used in a specific project of 240 m high power transition tower. However, as the request in terms of length capacity cannot be met by the testing labs in Belgium, the studies have concentrated on the profile made of L250x250x28 angles.

Firstly, a critical review of the current European normative documents (EN 50341, EN1993-1–3, prEN1993-3) has been made and the buckling resistance of the above-mentioned profile has been evaluated. Then, an experimental compression test has been performed for this member. The test has been complemented by a full non-linear finite element simulation by means of ANSYS software. Experimental, numerical and analytical results have been compared and discussed. Finally, conclusions were drawn considering the design of S460 star-battened members in compression. These studies are part of an ongoing project entitled "New steel" funded by Elia and ArcelorMittal and involving the University of Liège.

Published in : Structures (2023), vol. 58, 105274
DOI: 10.1016/j.istruc.2023.105274
Status : Postprint (Author's version)

1. Introduction

In the coming years, the transmission capacity of the high voltage grid will be increased due to the massive introduction of renewable energies on the network and the out phase of the use of carbon related energy sources. In order to face the challenges of this energy transition, the transmission capacity of high voltage lines and towers must be significantly increased. To achieve this, the existing conductors should be multiplied or replaced by bigger and higher grade ones and this has a direct impact on the structural stability of the towers. Designed to support a maximum weighted load of 100 T in 1970, the towers must now be able to support loads at least 80 % higher, due to an accumulation of (i) the higher conductor loads caused by the increase of their sections, (ii) the climate change that prescribes 20 % higher wind loads than in 1970, and (iii) the higher density of the residential areas that requires new towers up to 20 m higher so as to ensure sufficient safety clearance. Faced with these needs, the current networks look to be obsolete and their lattice towers must therefore be reinforced while new towers – in some cases extremely tall – need to be designed for higher loads, where built-up star-battened profiles may be used. The main advantage of these profiles is the high moment of inertia resulting from the distance between the centroids of the individual chords, which decreases the column's slenderness ratio and increases both the axial force and bending moment capacities.

Currently, all high voltage lattice towers are made of S355 steel grade, which was introduced in the early 1960s and is still used in new towers up to today. Being so, the design of the majority of towers is based on a steel quality that is no longer sufficient to meet the new higher structural performance requirements. Therefore, the use of high strength steel (HSS) is deemed necessary in order to meet the new structural performance requirements with the goal of minimum visual impact and CO_2 footprint [1,2]. Among them, S460 stands out with a yield strength up to 30 % higher than S355, while for the same structure and tower geometry, an S460 tower could carry higher loads. This solution fits with the request of power transport upgrade while minimising the need of human engineering resources and construction time, so as to conform with the climate agreement timeline. Moreover, the weight of an S460 tower could be reduced compared to its S355 counterpart by optimizing the section of the profiles, leading to lighter structures and thus also potentially reducing the size of foundations or the need to reinforce them. Therefore, S460 appears quite promising for the sustainable strengthening of existing towers and for the design of new ones that will contribute to the successful energy transition of the grid.

Lattice transmission towers in Europe are currently designed according to EN 1993-3-1 [3] with references when it is necessary to other parts of Eurocode 3 such as EN 1993-1-1 [4], EN 1993-1-5 [5] and EN 1993-1-8 [6], or in accordance with the CENELEC standard EN 50341-1 [7] which is exclusively dedicated to the design of overhead electrical transmission lines. For some aspects, however, the design methods given in the latter diverge from the rules provided in the Eurocodes as discussed in Ref. [8]. Additionally, even if this is not strictly prohibited, the application of EN 50341 to S460 steel grades remains quite questionable, as the normalisation of S460 steel within the standard EN 10025 [9] for hot-rolled products is more recent (2019) than the last revision of EN 50341 (2012). It is also remarkable that amongst all these normative documents, a number of inconsistencies have been identified, concerning different aspects of design as addressed in detail in Ref. [10]. Although new steels have been developed recently, the lack of evolution concerning their use in electrical pylons is

Published in : Structures (2023), vol. 58, 105274
DOI: 10.1016/j.istruc.2023.105274
Status : Postprint (Author's version)

due to the slow evolution of the extremely strict normative context to which the dimensioning, fabrication and production of steel structures (EC3) and in particular steel structures for overhead electrical lines (EN 50341) are subjected. However, in the framework of the recently finished European RFCS- supported project ANGELHY [11], existing European specifications on single and star-battened angle sections were reviewed, experimental, analytical and numerical studies were conducted and a complete set of design rules for pin-ended members considering steel grades up to S460 has been developed. The proposed design rules have been included nowadays as Annex F in the latest version of prEN 1993-3 [12]. However, they are not accounting for the effects of the restraints generated by the bolted connections at the extremities of the members.

Extensive research has been carried out in the recent years to study the behaviour of single or built-up sections made of angle profiles, but focusing mainly on regular steel grades. Schillo et al. [13] examined the rules of the European standards discussed before (i.e EN 1993-1, EN 1993-3, EN 50341-1) concerning the buckling resistance of S355 rolled angles and compared them to test results and numerical investigations considering various types of initial imperfections. Bezas et al. [14,15] proposed a complete and duly validated set of design rules for pin-ended angles covering all aspects of their design (classification, cross-section and member resistance); these rules were validated for high strength steel S460 too and are included in prEN 1993-3. Timošenko [16] studied theoretically the resistance of built-up battened columns but with much higher distances between the members. Beyer et al. [17] performed a numerical sensitivity analysis on different parameters (distance of packing plates, clearance of the bolt holes etc) related to the geometry of built-up S355 members. More recently, Saufnay et al. [18] investigated experimentally and numerically the behaviour of closely spaced built-up star-battened angles members made of S355 equal and unequal angle profiles. Kayser et al. [19] investigated numerically the behaviour of welded star-battened angles columns made of stainless steel, while Behzadi et al. [20] studied the behaviour an design of cruciform steel columns. Further experimental studies of closely spaced built-up members can be found in Ref. [21–23], but none of them was referring to high strength steel.

This paper focuses on the buckling resistance of a star-battened member constituted of large angle sections made of HSS. Firstly, a critical review of the current European normative documents such as EN 50341, EN1993-1-3 as well as its latest version prEN1993-3 has been made. In order to make more concrete comparisons between the standards, a star-battened member made of two S460 L250x250x28 angles that is subjected to pure compression has been considered as case study, and its buckling resistance has been evaluated using the provisions of all the above-mentioned standards. The member of the case study has also been tested experimentally, since Annex J of EN 50341 requests an experimental validation. Geometrical imperfections and material properties, including residual stresses, were also measured. In addition, the experimental test has been complemented by a full non-linear finite element numerical simulation by means of the Ansys software [24], considering actual material and geometrical non-linearities. Experimental, numerical and analytical results have been compared and discussed. Furthermore, the present work intends to proof analytically, experimentally and numerically that a star-battened member made of two S460 L300x300x35 angles with a 4486 mm length exhibits a required capacity of about 15,0 MN, for its application in a specific project of 240 m high power transition tower. If the target resistance is reached, this would result in a benefit of 60 % in design time, 50 % in production time and 50 % in weight (reduced CO_2 footprint). However, as the

Published in : Structures (2023), vol. 58, 105274
DOI: 10.1016/j.istruc.2023.105274
Status : Postprint (Author's version)

request in terms of length capacity cannot be met by the testing labs in Belgium, the studies have concentrated on the profile made of L250x250x28 angles, with an adapted length to create a comparable stress situation. Finally, conclusions were drawn considering the design of S460 star-battened members in compression and so for the targeted member made of L300x300x35 angles.

These studies presented in this paper are part of an ongoing project entitled "New steel" funded by Elia and ArcelorMittal industrial partners and involving the University of Liège.

Nomenclature

Latin upper-case symbols

A, A_{eff}	gross and effective area of a cross-section, respectively
A_s	stress area of a bolt
E	modulus of elasticity
G	shear modulus
I_T	De Saint-Venant torsional constant
I_W	warping constant
$I_{v,ch}$	moment of inertia about its minor axis for one angle profile
$I_{i,SB}$	moment of inertia of the star-battened profile about its i axis
L	length (member length, span length etc.)
L_{cr}	buckling length
$N_{b,Rd}$	design value of the buckling resistance of a member in compression
$N_{c,Rd}$	design value of the resistance to uniform compression axial force of the cross-section
N_{cr}	elastic critical axial force for the relevant buckling mode based on the gross cross-sectional properties
$N_{cr,Sv}$	elastic critical axial force considering of the effect of the shear stiffness
N_{Rk}	characteristic value of the resistance to axial force
N_{ult}	ultimate test resistance to axial force of the cross-section
S_v	shear stiffness of the member

Latin lower-case symbols

$\bar{b}$	appropriate width that is equal to h for angle sections according to EN1993-1-5
c	outstand flange width (c = h-t-r)
f_y	yield strength
h	width of the cross-section
h_0	distance between the centroids of the two individual angle sections
i_i	radius of gyration about i axis
k_σ	plate buckling coefficient
m	number of angles for the compound member check acc. to EN50341
r	radius of root fillet
r_o	polar radius of gyration
t	thickness of the cross-section

Greek lower-case symbols

α	imperfection factor, distance between battened plates
γ_{M0}	partial factor for resistance of cross-sections that equals 1,0 as recommended by EN1993-1-1
γ_{M1}	partial factor for resistance of members to instability assessed by member checks that equals 1,0 as recommended by EN 1993-1-1
ε	material parameter depending on f_y, equals $\varepsilon = \sqrt{235/f_y\left[\frac{N}{mm^2}\right]}$
$\bar{\lambda}$, $\bar{\lambda}_{eff}$	relative or effective slenderness
$\bar{\lambda}_p$	relative plate slenderness for plate buckling
ρ	reduction factor for plate buckling
χ	reduction factor due to relevant buckling mode

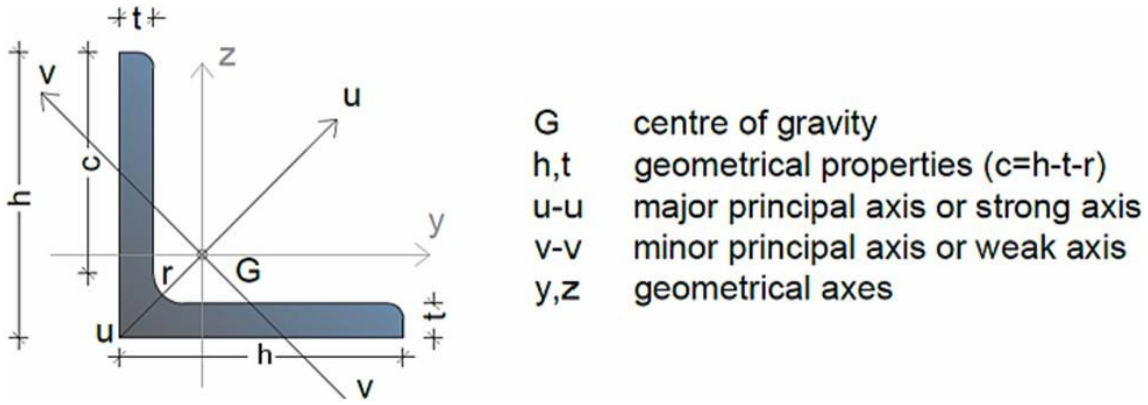

Fig. 1. Notations for geometrical properties and axes.

Published in : Structures (2023), vol. 58, 105274
DOI: 10.1016/j.istruc.2023.105274
Status : Postprint (Author's version)

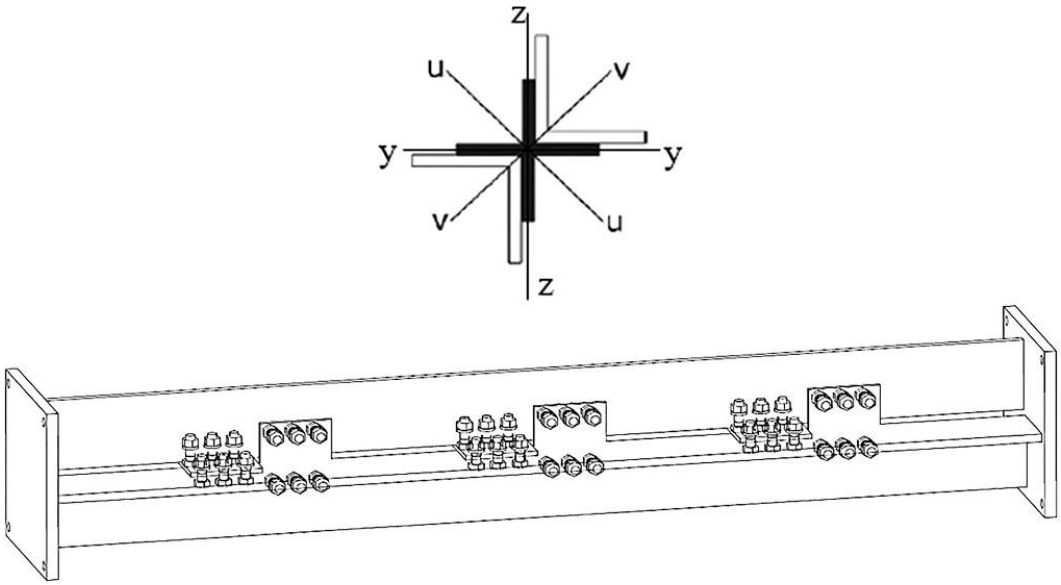

Fig. 2. General layout of the member and definition of axes.

Table 1
Built-up star-battened cross-section properties.

Property	Value	
Area A_{SB}	26,600	mm^2
Moment of inertia $I_{max,SB} = I_{u,SB}$	40,586	cm^4
Radius of gyration $i_{max,SB} = i_{u,SB}$	123,5	mm
Radius of gyration $i_{min,SB} = i_{v,SB}$	95,4	mm
Radius of gyration $i_{x,SB}$	110,4	mm
Torsion constant $I_{T,SB}$	$6{,}908 \cdot 10^5$	mm^4
Warping constant $I_{w,SB}$	$3{,}206 \cdot 10^6$	mm^6

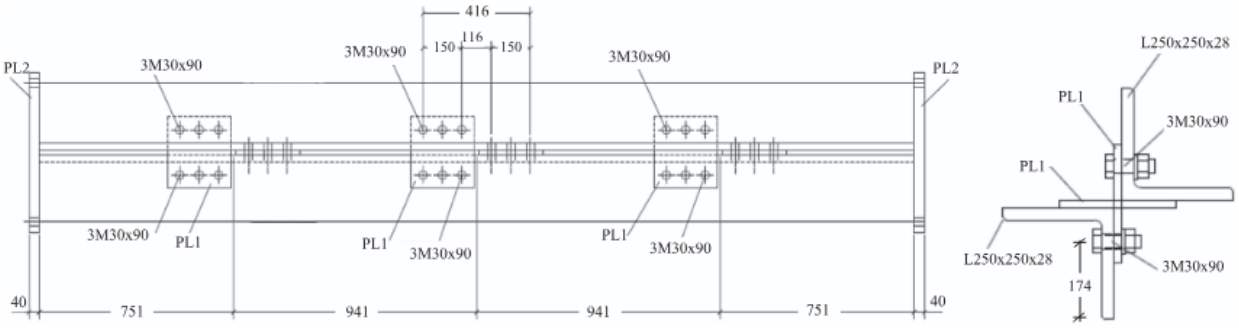

Fig. 3. Geometry of the studied member.

Published in : Structures (2023), vol. 58, 105274
DOI: 10.1016/j.istruc.2023.105274
Status : Postprint (Author's version)

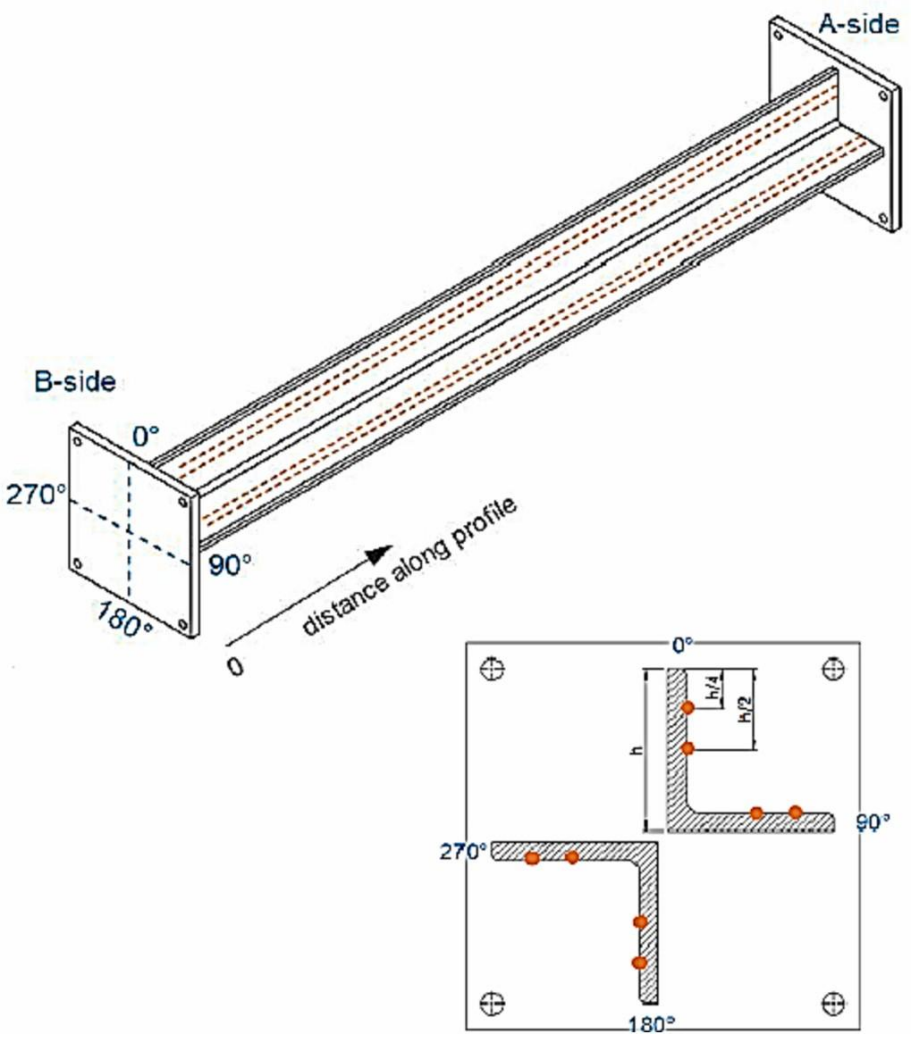

Fig. 4. Definition of the out-of-straightness measurements paths.

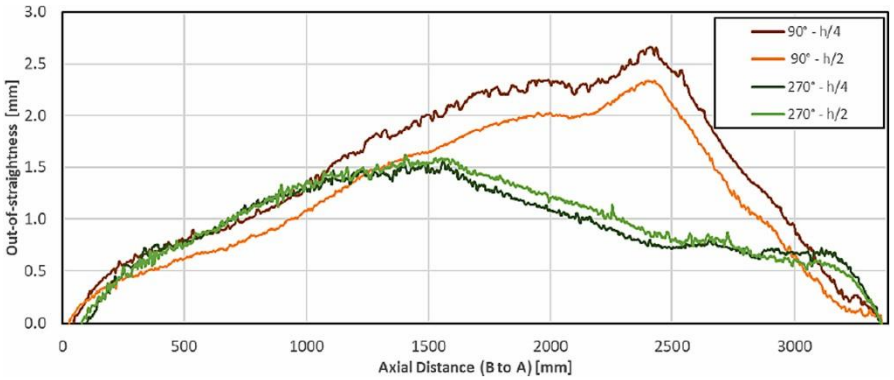

Fig. 5. Straightness measurements in plane 90°-270°.

Published in : Structures (2023), vol. 58, 105274
DOI: 10.1016/j.istruc.2023.105274
Status : Postprint (Author's version)

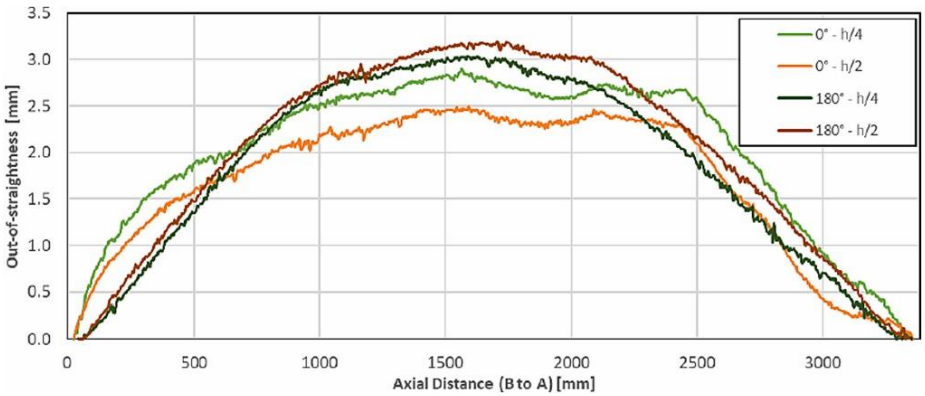

Fig. 6. Straightness measurements in plane 0º-180º.

2. Critical review of the existing normative documents

As already mentioned in the introduction, the normative documents under concern of this paper are (i) EN 50341, (ii) EN 1993-3-1 and (iii) prEN 1993-3. As two over three partners of this project (Elia & ULiège) are located and act in Belgium, it has been decided to follow also the relevant National Annexes of Belgium when it is necessary (i.e [25;26] for EN 50341 and EN 1993-3-1 respectively). In the following, the design rules for cross-section classification as well as cross-section and member resistance for star-battened members subjected only to axial compression are addressed and discussed.

2.1. CLASSIFICATION AND CROSS-SECTION RESISTANCE

Due to the loading condition, only the limit between Class 3 and 4 needs to be defined. The cross-section design resistance of a star- battened member for axial compression is given, according to all examined standards, by:

$$N_{c,Rd} = \begin{cases} \dfrac{2Af_y}{\gamma_{M0}} & \text{for class 1, 2 and 3 profiles} \\ \dfrac{2A_{eff}f_y}{\gamma_{M0}} & \text{for class 4 profiles} \end{cases} \qquad (1)$$

where A and A_{eff} is the gross and the effective cross-section area of one angle profile; the discussion hereafter will be limited to the evaluation of its effective area.

2.1.1. EN 50341

In §7.3.6.2 of EN 50431, for the boundary between Class 3 and Class 4 sections, reference is made to §5.5 of EN 1993-1-1 in which two limits are provided, according to the sheet to which one refers in Table 5.2 (see **Fig. 1** for the notations):

- $h/t \leq 11{,}5\varepsilon$ (Sheet 3 of 3)

Published in : Structures (2023), vol. 58, 105274
DOI: 10.1016/j.istruc.2023.105274
Status : Postprint (Author's version)

- $c/t \leq 14{,}0\varepsilon$ (Sheet 2 of 3) which is approximatively equivalent to $h/t \leq 17{,}5\varepsilon$ by assuming approximately $c = 0{,}8h$.

At first, it must be noted that, surprisingly, both criteria are not based on the same geometrical properties (i.e. h and c). Secondly, it can be observed that the Sheet 3 criterion is the governing one.

For the determination of the class-4 cross-section resistance, a reduced area (A_{eff}) should be evaluated according to the procedure described in EN 1993-1-5, as requested by EN 1993-1-1. This procedure requires the definition of a reduction factor ρ for local buckling, that may be obtained for outstand plated elements as follows:

$$\rho = \begin{cases} 1{,}0 & \text{for } \bar{\lambda}_p \leqslant 0{,}748 \\ \dfrac{\bar{\lambda}_p - 0{,}188}{\bar{\lambda}_p^2} & \text{for } \bar{\lambda}_p > 0{,}748 \end{cases} \qquad (2)$$

where:

$$\bar{\lambda}_p = \frac{\bar{b}/t}{28{,}4\varepsilon\sqrt{k_\sigma}} \qquad (3)$$

and in which $\bar{b}/t$ is the ratio between the width of the plate and its thickness.

It should directly be noted that the definition of ρ is unique, while the classification criteria differ according to the used sheet of the table (Sheet 2 or Sheet 3). In fact, the definition of ρ in EN 1991-1-5 is only adapted to the Sheet 2 classification criterion (classification of the legs as "outstand" plate elements). This may be easily shown through the following reasoning:

- At the limit between Class 3 and Class 4, $\rho = 1$ and therefore $\lambda_p = 0{,}748$;
- In table 4.2 of EN 1993-1-5, the buckling factor for outstand elements in compression ($\psi = 1$) is defined as $k_\sigma = 0{,}43$. Then through Eq.3, it can be found that $\lambda_p = 0{,}748$ corresponds to a $\bar{b}/t$ value equal to $13{,}9\varepsilon \approx 14{,}0\ \varepsilon$, i.e. the boundary value provided in Sheet 2 if $\bar{b}$ is taken equal to c;
- But EN 1993-1-5 recommends selecting $\bar{b}$ as equal to h for angle sections, and not to c, so it is introducing a clear contradiction between EN 1993-1-1 and EN 1993-1-5.

Therefore, it is quite impossible to find a reasonable interpretation of these two normative documents for the classification of angle cross-sections, and therefore also of EN 50341 (even if, in the latter, a quite better definition of the $\bar{b}$ value is proposed; it is set to use the value $h - 2t$ that is in accordance with EN 1993-3-1).

Published in : Structures (2023), vol. 58, 105274
DOI: 10.1016/j.istruc.2023.105274
Status : Postprint (Author's version)

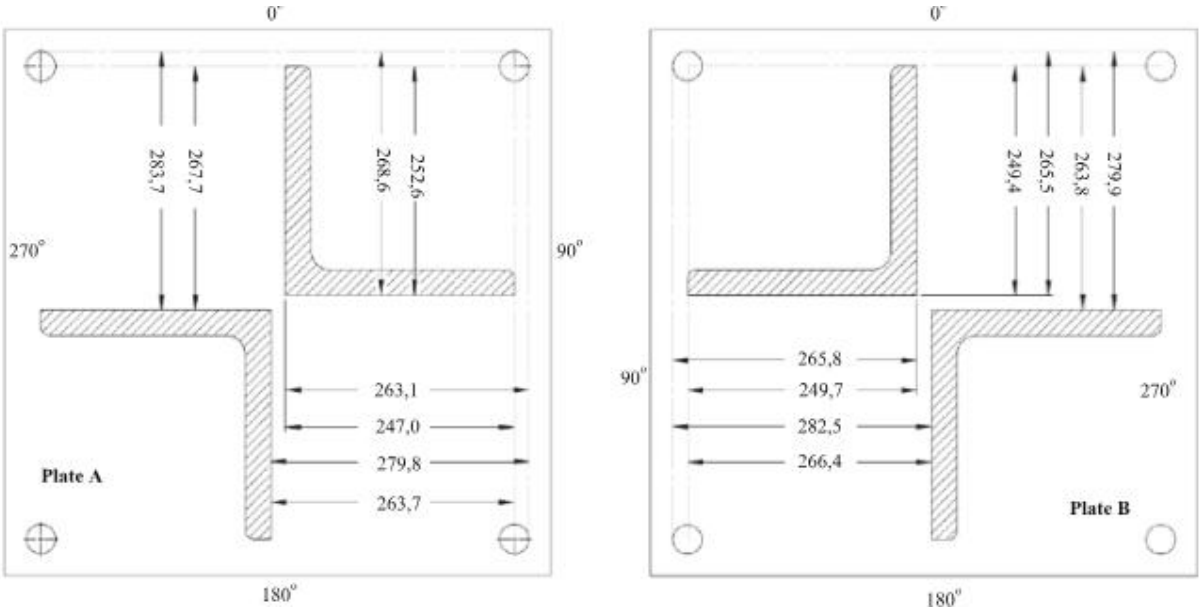

Fig. 7. Measured eccentricities at the endplates.

Table 2
Actual dimensions of the cross-sections.

Position of measurement	Thickness [mm]	Width [mm]
A 0°	27,6	253,3
A 90°	27,7	255,0
A 180°	27,8	254,9
A 270°	27,7	254,4
B 0°	27,6	254,7
B 90°	27,9	254,9
B 180°	27,6	254,7
B 270°	27,6	254,7
Mean values	27,7	254,6

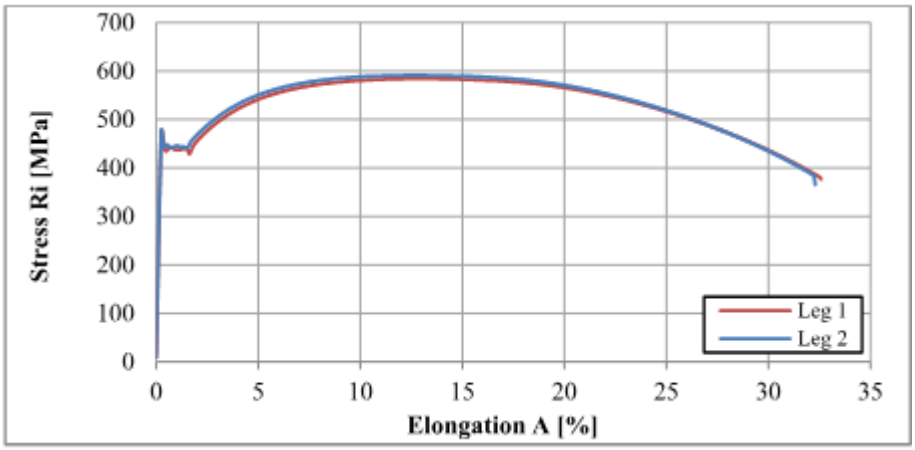

Fig. 8. Stress–strain curves from the coupon tests.

Published in : Structures (2023), vol. 58, 105274
DOI: 10.1016/j.istruc.2023.105274
Status : Postprint (Author's version)

Table 3
Coupon test's results.

	R_{eH} [MPa]	R_{eL} [MPa]	R_m [MPa]	E [N/mm^2]
Leg 1	477,3	444,5	584,1	214,617
Leg 2	479,7	445,6	591,2	211,025
Mean value	478,5	445,0	587,6	212,821

2.1.2. EN 1993-3-1

A similar procedure that in EN 50341 is globally recommended in EN 1993-3-1. The classification of cross-sections should follow the provisions of EN 1993-1-1, but here it is clearly indicated that the maximum width to thickness ratio for angles defined in **Table 5.2** of EN 1993-1-1 may be taken as the ratio *(h-2 t)/t*, instead of h/t. The value *(h-2 t)/t* is not equal but quite close to *c/t* used in Sheet 2 of EN 1993-1-1; on the contrary, to replace *h/t* by *(h-2 t)/t* in Sheet 3 of EN 1993-1-1 leads to a classification criterion *(h-2 t)/t ≤ 11,5* which seems to be optimistic. The reduction factor ρ is then again provided by Eq.2 and Eq.3, using $\bar{b} = h - 2t$. This modification reintroduces some consistency between EN 1993-1-5 and EN 1993-1-1 Sheet 3 which is the main reference for the classification of angles sections.

2.1.3. prEN 1993-3

In the ANGELHY project [11], it has been demonstrated that the Sheet 3 criterion was not at all relevant for angle sections in compression, and so should be disregarded. The only criterion that should be applied is the one described in Sheet 2, i.e. $c/t \leq 14{,}0\varepsilon$, with $c = h - t - r$. The numerical and analytical background and validations of these rules may be found in Ref. [14].

Following the recommendations of ANGELHY, prEN 1993-3 recommends presently in its Annex F to refer only to EN 1993-1-1 **Table 5.2** Sheet 2, and no more to Sheet 3, but adopts, as it was already the case in the previous draft, $\bar{b} = h - 2t$, so the criterion is expressed as $(h-2t)/t \leq 14{,}0\varepsilon$.

If the evaluation of the reduction factor ρ given by Eq.2 and Eq.3 is also based on ~~b~~ $= h - 2t$, then a full compatibility is reached between the classification criterion and the rules provided for angle cross-section resistance.

2.1.4. SUMMARY

The recommendations provided in prEN 1993-3 allow a full consistent determination of the cross-section class and of the cross-section resistance (according to EN 1993-1-5), in contradiction to the rules recommended by EN 50341 and EN 1993-3. They are also in full compliance with the conclusions drawn in the ANGELHY European project, the only difference lying in the way on how the plate width ~~b~~ is defined, respectively equal to $c = h-t-r$ in the ANGELHY project and $h-2\,t$ in prEN 1993-3, but this difference is quite negligeable in practical cases. Further comparisons regarding the classification criteria of the available standards can be found in Ref. [14].

Published in : Structures (2023), vol. 58, 105274
DOI: 10.1016/j.istruc.2023.105274
Status : Postprint (Author's version)

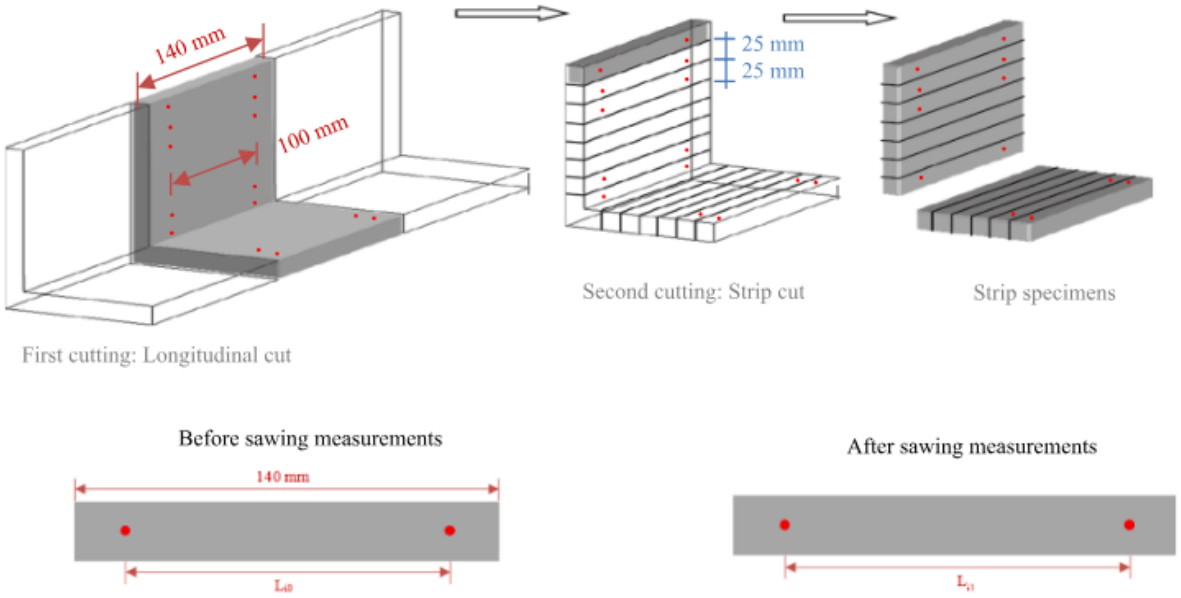

Fig. 9. Schematization of the sectioning method's steps and notations of the measurements.

2.2. BUCKLING RESISTANCE TO COMPRESSION

2.2.1. EN 50341

In the CENELEC document EN 50341, it is stated that compression members shall be designed using the provisions of Annex G and Annex H of EN 1993-3-1, or in accordance with the provisions of Annex J.4 of EN 50341, only if full-scale tests are performed. For the latter, it is also indicated in §7.3.9 that the experimental resistance should be at least 5 % higher than the analytically determined design load for the ultimate limit state.

Besides that, even if this is not strictly prohibited, the application of EN 50341 to S460 steels remains questionable as also explained in the introduction; in different places in the document, specific rules are provided for S235 and S355 steels, but not for S460. This being, Annex J.4 will anyway be applied here below, for comparison with the other design procedures, and this application will be complemented by an experimental test.

According to Annex J.4, the design buckling resistance of a compression member should be taken as:

$$N_{b,Rd} = \begin{cases} 2\chi A f_y/\gamma_{M1} & \text{for Class 1, 2 and 3 cross - sections} \\ 2\chi A_{eff} f_y/\gamma_{M1} & \text{for Class 4 cross - sections} \end{cases} \quad (4)$$

where A and A_{eff} is the gross and the effective cross-section area of one angle profile.

The reduction factor χ is determined as a function of the effective slenderness $\bar{\lambda}_{eff}$, which is evaluated for the relevant buckling mode, i.e. for a flexural buckling mode (index *F*) about v-v or u-u axis - see **Fig. 2** for the definition of these axes – or a torsional buckling mode (index *T*), as the member cross-section shown in **Fig. 2** being a double symmetrical one. Additionally, a specific formula for the calculation of the slenderness of compound members is also provided in J.4.3.4.3 (index *u*) which

Published in : Structures (2023), vol. 58, 105274
DOI: 10.1016/j.istruc.2023.105274
Status : Postprint (Author's version)

should be considered for the design. Therefore, $\bar{\lambda}_{eff}$= max{$\bar{\lambda}_{eff,F}$, $\bar{\lambda}_{eff,T}$, $\bar{\lambda}_{eff,u}$}. For all the above-mentioned cases, the imperfection factor α should be taken for buckling curve a_0 = 0,13 (former 0,125 value).

2.2.2. EN 1993-3-1

As in EN 50341, reference is also made to Annexes G and H in EN 1993-3-1. The design buckling resistance is given by Eq.4, while the reduction factor χ is again determined as a function of the effective slenderness $\bar{\lambda}_{eff}$, which is evaluated again for the relevant buckling mode. Here however, the specific check for compound members is not addressed; subsequently $\bar{\lambda}_{eff}$= max{$\bar{\lambda}_{eff,F}$, $\bar{\lambda}_{eff,T}$}. Furthermore, the imperfection factor α should be taken as equal to 0,34 for angle sections according to EN 1993-1-1, and so it corresponds to buckling curve *b*.

2.2.3. prEN 1993-3

The resistance of closely spaced built-up members is checked according to EN 1993-1-1 for flexural buckling about both principal axes using buckling curve *b*. The slenderness of star battened members for flexural buckling about the u-u axis may be given by:

$$\bar{\lambda}_{Sv} = \sqrt{\frac{N_{Rk}}{N_{cr,Sv}}} \qquad (5)$$

while buckling about v-v axis is evaluated as for the other two considered normative documents. For the latter, index F will be further used in order to be in line with the notations used in the previous sub-sections. For the former, even though it represents a flexural buckling about the strong axis, the index S_v will be used so as to be in line with the notation given in prEN 1993-3, Annex F. In this case, S_v indicates that the shear stiffness is accounted for when calculating the critical axial force.

The critical axial force of the built-up member $N_{cr,Sv}$ considering the effect of the shear stiffness may be determined as follows:

$$N_{cr,Sv} = \frac{1}{\frac{1}{N_{cr}} + \frac{1}{S_v}} \qquad (6)$$

where N_{cr} is the critical axial force of the built-up member considered as integral neglecting the influence of the shear stiffness, i.e.

$$N_{cr,u} = EI_{u,SB}\left(\frac{\pi}{L_{cr}}\right)^2.$$

The shear stiffness of the built-up member S_v is depending on the connection type. For star-battened members connected with fit bolts may be given by $S_v = \frac{1}{\frac{a^2}{24EI_{v,ch}} + \frac{a}{h_0 GA_s}}$ where a is the distance between the connections of the built-up member. The calculation of the shear stiffness of members connected through preloaded bolts, non-fully preloaded bolt connections or other built-up configurations, is described in Ref. [12].

Published in : Structures (2023), vol. 58, 105274
DOI: 10.1016/j.istruc.2023.105274
Status : Postprint (Author's version)

For the determination of the reduction factor χ, the slenderness should be taken as $\bar{\lambda}_{max} = \max\{\bar{\lambda}_{Sv}, \bar{\lambda}_F\}$. It has been shown in the framework of the ANGELHY project [27] that torsional or flexural–torsional modes are not relevant for star-battened profiles fabricated from hot-rolled angle sections, as it has been shown also for hot-rolled single angle pin-ended sections [10]. This observation has been validated experimentally and numerically over the whole member buckling slenderness range, covering thus values of the relative slenderness between 0, 2 and 0,4. Nonetheless, as has been shown analytically in Ref. [27] for very high values of the cross-section slenderness (b/t ratio) torsional buckling modes may arise. These failure modes may be covered by the local buckling check as proposed in ANGELHY project [11]. This can be justified as torsional buckling modes are mechanically very similar to local buckling modes in the case of the studied section as has also been discussed in Ref. [20].

2.2.4. COMPARISON OF THE STANDARDS

EN 50341:2012 Annex J looks to provide a quite advantageous evaluation of the χ factor, but also quite questionable. The use of curve a_0 for buckling about the u-u axis (with an imperfection factor of 0,13) is quite optimistic and could never be scientifically justified, as it has been shown in the ANGELHY project [11]. But on the other hand, it is based on an evaluation of the relative slenderness where flexural–torsional effects have been accounted for. Being so, EN 50341 leads to a safe estimation of the relative slenderness, which is further compensated by the unsafe selection of curve a_0. Moreover, curve a_0 applies also in EN 50341 for buckling about the v-v axis. This is again quite surprising as this buckling mode is the one of two simple independent angles, for which, even EN 1993-1-1: Table 6.2 recommends curve *b*. This raises another contradiction in EN 50341, in addition to the classification aspects. Finally, although the provisions of this standard are based on numerous experimental full-scale tests on pylons, those were made of S235 and S355 steel, and so the extrapolation of the standard to higher steel grades without further investigations cannot be contemplated.

Compared to EN 50341, the application of EN 1993-1-1 leads to lower resistance as a consequence of the combination of (i) the use of curve b and (ii) the consideration of flexural–torsional detrimental effects.

In prEN 1993-3 Annex F, curve b is used for buckling about u-u and the v-v axes (imperfection factor of 0,34) but is based on a relative slenderness in which torsional and flexural–torsional aspects are not considered [28]. This approach, including the classification of angle cross-sections, has been numerically and experimentally validated within the ANGELHY project. It should be mentioned that both, the design procedure of prEN1993-3 and the compound member check of EN 50341, also known as the modified slenderness ratio approach, are based on the same analytical background provided by Timoshenko [29]. Despite its ease of use, the modified slenderness method is neither accounting for the fact that members are very closely spaced and consequently the influence of the battens eliminates, neither for the type of the connection (preloaded bolts, non-preloaded bolts, etc). Some extensions of the modified slenderness concept have been proposed in Ref. [30] to account for the connection by introducing additional factors; the rules provided in prEN 1993-3 also consider these effects. Furthermore, the design procedure of prEN1993-3 aims to not transform the critical axial forces to modified values of the slenderness but to conserve a critical axial force accounting for the shear flexibility. Then, in future step, interaction equations accounting for axial forces and bending

Published in : Structures (2023), vol. 58, 105274
DOI: 10.1016/j.istruc.2023.105274
Status : Postprint (Author's version)

moments may be easily adapted to built-up members as these equations often use critical axial forces as one parameter.

Therefore, the use of prEN 1993-3 appears today the only fully consistent and validated normative approach (amongst the three considered standards of this paper) to estimate the buckling capacity of a pinned built-up star-battened member made of S460 steel.

Fig. 10. Steps of the sectioning method for the tested profile: (a) mark of the specimens and reference points (left), (b) longitudinal sawing (middle), and (c) strip specimens (right).

3. Case study

To draw solid conclusions on the analysed norms, a profile has been selected as a case study and its buckling resistance has been evaluated experimentally, numerically and analytically.

3.1. DETAILS OF THE STUDIED MEMBER

The cross-section of the member consists of two L250x250x28 angle profiles made of S460 steel grade, as shown in **Fig. 2**. The L-profiles are interconnected by 6 plates (PL1 = 246x264x16 mm) using non-preloaded bolts M30x90 (8.8), while they are welded at their extremities to end plates (PL2 = 596x596x40 mm). Nevertheless, in real transmission towers those end plates are not met in the main legs, the continuity of these ones being assured by means of splice connections along the tower's height. In the tested specimen, the continuity of the leg has been simulated through welded end plates (i.e. equal stress distribution and free rotation at the extremities – see **section 3.2.2.1** for the applied boundary conditions during the test). It should be also mentioned that the nature of the connections (bolted/welded) is not influencing a lot the response of the member, as long as the connections possess a sufficient rotational stiffness.

The nominal total member length (including the end plates) equals L = 3464 mm while the distance between the intermediate connection plates is 941 mm, as illustrated in **Fig. 3**. The advantage of keeping the bolted rows near to the centre of the assembled profile is to limit the shear forces in the

Published in : Structures (2023), vol. 58, 105274
DOI: 10.1016/j.istruc.2023.105274
Status : Postprint (Author's version)

interconnection plates resulting from the buckling of the individual angle members. Indeed the more the bolt row is placed far from the central axe, the higher are the internal moments in the bolted connections. And these internal loads within the interconnection plates are introducing secondary stress moments around the outer borders of the single members at the level of these interconnections. These reasons are justifying the positioning of the bolt rows so close to the heels of the angle profiles.

Table 1 summarizes the geometrical properties of the star-battened built-up section (indicated with the index SB) that are required for the calculation of the member resistance.

According to the normative document EN 10025 [9] for hot-rolled products, the minimum yield strength f_y for the considered cross-section made of steel grade S460 equals 440 MPa (and $\varepsilon = \sqrt{235/f_y}$ = 0,731). This reduction results from the 28 mm thickness of the angles. In EN 50341, EN 1993-3 and prEN 1993-3, which all refer to EN 1993-1-1, an alternative variation of the yield strength with the plate thickness is suggested in which no reduction of the yield strength is recommended for thicknesses lower than 40 mm. The use of these thickness variation laws can be set in the National Annexes. In Belgium [31], reference must be made to product norm EN 10025, and a yield strength of 440 MPa is therefore adopted here. Afterwards, three situations have been considered for sake of comparison; the first two cases adopt the nominal values of the material properties (i.e. f_y = 440 MPa, f_y = 460 MPa, E = 210000 N/mm^2) while the third one follows the actual measured material properties (see **section 3.2.1.2**).

3.2. EXPERIMENTAL TEST

The experimental test of the specimen described in **section 3.1** is presented in this section. Its associated measurements such as initial imperfections and material properties are also reported, but more details can be found in Ref. [32,33]. The buckling test has been carried out at OCAS NV (ArcelorMittal Global R&D Gent) while some of the associated measurements have been performed by the "Laboratoire de M´ecanique des Materiaux et Structures´ " of Liege University. `

3.2.1. ASSOCIATED MEASUREMENTS

3.2.1.1. Initial imperfections. The initial imperfections – sample's straightness and eccentricities of endplates – have been measured through a 3D scan, using a Handyscan 3D-700 portable scanning system. The sample has been cleaned by removing the loose scale chips from the surface of the L-profiles and then reflective dots were pasted on its surfaces. Separate scans were made for the endplates and the individual L-profiles with 1 mm resolution. The measurement accuracy of the scans of the L-profiles was 0.12 mm while of the endplates was 0,08 mm.

The imperfections were measured along 8 different paths. More precisely, two measurements have been taken on each internal face of both profiles, one at the mid height (h/2) and a parallel track at h/4 as illustrated with orange dot lines in **Fig. 4**; the notations and the orientations (0°_90°_180°_270°) of the planes are also shown in this figure. **Fig. 5** and **Fig. 6** present the measurements taken in the 90°-270° and in the 0°-180° plane, respectively. For the former, the maximum measured out-of-straightness is 2.7 mm while for the latter equals 3.2 mm. It can also be seen that, as expected, the lines referring to the same face of the profile have the same overall trend. Additionally for all profiles

Published in : Structures (2023), vol. 58, 105274
DOI: 10.1016/j.istruc.2023.105274
Status : Postprint (Author's version)

the maximum imperfections are at their mid-length, but for one face (90°-h/2 and 90°-h/4) are closer to the quarter length.

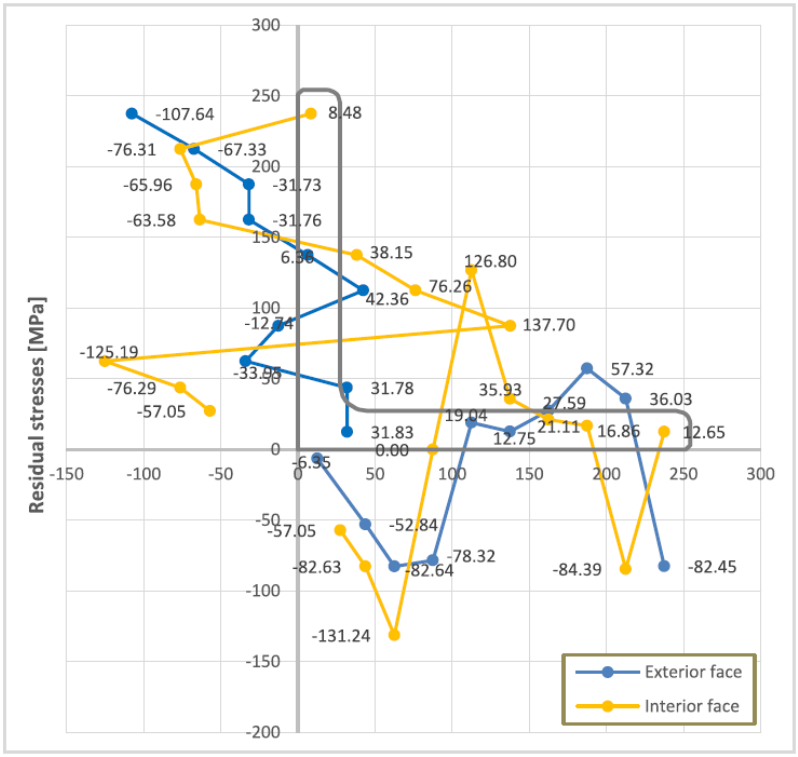

Fig. 11. Residual stresses of the angle profile L250x28 for both faces (interior/exterior).

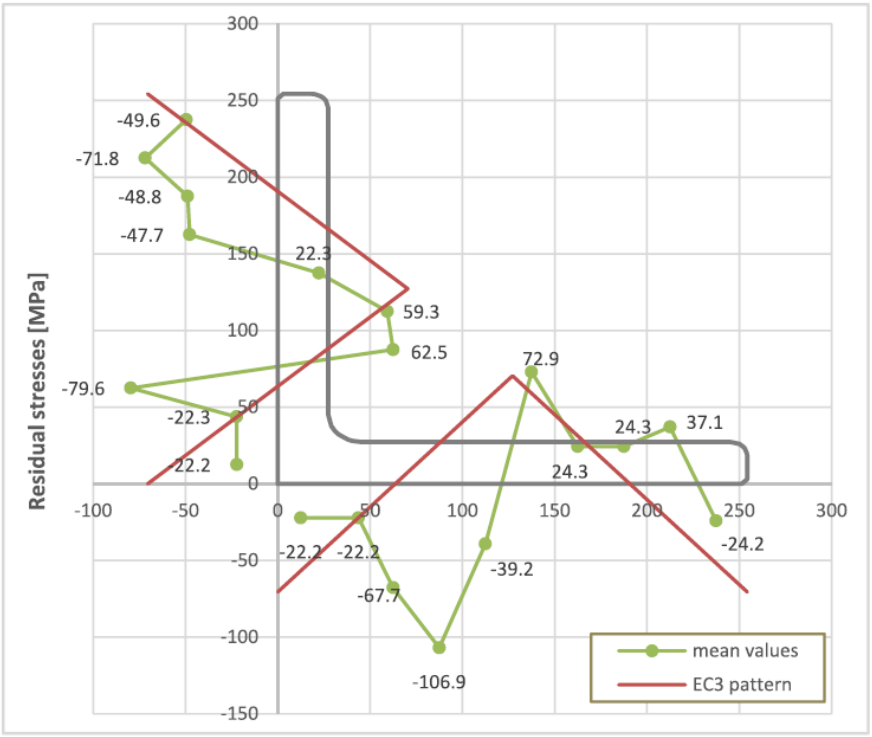

Fig. 12. Mean values of the residual stresses of the angle profile L250x28 and comparison with the pattern proposed by Eurocode 3.

Published in : Structures (2023), vol. 58, 105274
DOI: 10.1016/j.istruc.2023.105274
Status : Postprint (Author's version)

Fig. 13. Buckling specimen installed in the test rig.

Furthermore, measurements have been performed in order to determine the exact position of the specimen on its end plates and to identify a possible eccentricity at which the compression force would be applied in the testing machine. They are summarized in **Fig. 7** for both extremities. The measured misalignment was compensated for when mounting the specimen to the swivel joint of the test rig. This procedure was aimed to reduce the final eccentricity of the mounted sample to 0,3 mm.

In order to determine the actual cross-section dimensions, measurements have been performed close to both extremities of the specimen (see **Fig. 7** for the determination of the notations). The values are reported in **Table 2**. It can be seen that the differences with the nominal values (L250x250x28) are quite small (2 % for the width and 1,4% for the thickness).

3.2.1.2. Coupon tests. Coupon tests have been performed in accordance with ISO 6892-1:2016 [34]. Two samples have been extracted from one of the angle profiles, one from each leg. **Fig. 8** shows the stress–strain curves obtained from both tensile tests, while **Table 3** provides their characteristic values. The stress R_{eH} refers to the upper value of the yield stress, while R_m to the ultimate strength. The yield strength f_y (engineering stress) may be determined by the mean value of the yield plateau of both curves and it is 445,0 MPa.

3.2.1.3. Measurements of the residual stresses. The determination of the residual stresses has been performed with the sectioning method, which is schematized in **Fig. 9**, where the stresses are evaluated by cutting the profile into longitudinal strips (of 140x25 mm) and measuring their length difference. The method is based on the principle that internal stresses are relieved by cutting the specimen into many strips of smaller cross-section area. Measurements have been performed for each strip in both interior and exterior face of the profile. By assuming that the transversal stresses are negligible, the simplified Hook's law may be applied. Therefore:

$$\sigma_{res,i} = E_{mean} \cdot \varepsilon_{res,i} = -E_{mean} \cdot (L_{i1} - L_{i0}) / L_{i0} \qquad \text{(Eq.7)}$$

Published in : Structures (2023), vol. 58, 105274
DOI: 10.1016/j.istruc.2023.105274
Status : Postprint (Author's version)

where L_{i0} and L_{i1} are determined in **Fig. 9**. **Fig. 10** illustrates the different cutting steps of the sectioning method for the tested profile.

Fig. 11 illustrates the measured residual stresses of the angle profile for both faces (interior/exterior). The significant differences in some points between the exterior and interior stresses have been observed in previous similar studies (see Ref. [35]), too. **Fig. 12** presents the mean values of both faces (i.e. $\sigma_{res,mean,i} = (\sigma_{res,Ei} + \sigma_{res,Ii})/2$). The pattern used for the background calculations of Eurocode 3 rules and proposed in Ref. [36], is also reported with an absolute maximum value equal to 0,3·235 MPa = 70,5 MPa, as the residual stresses of hot-rolled profiles are independent of the steel grade of the section. It can be seen that the maximum measured stresses and the normative ones are quite close while the global tendency of both curves is similar.

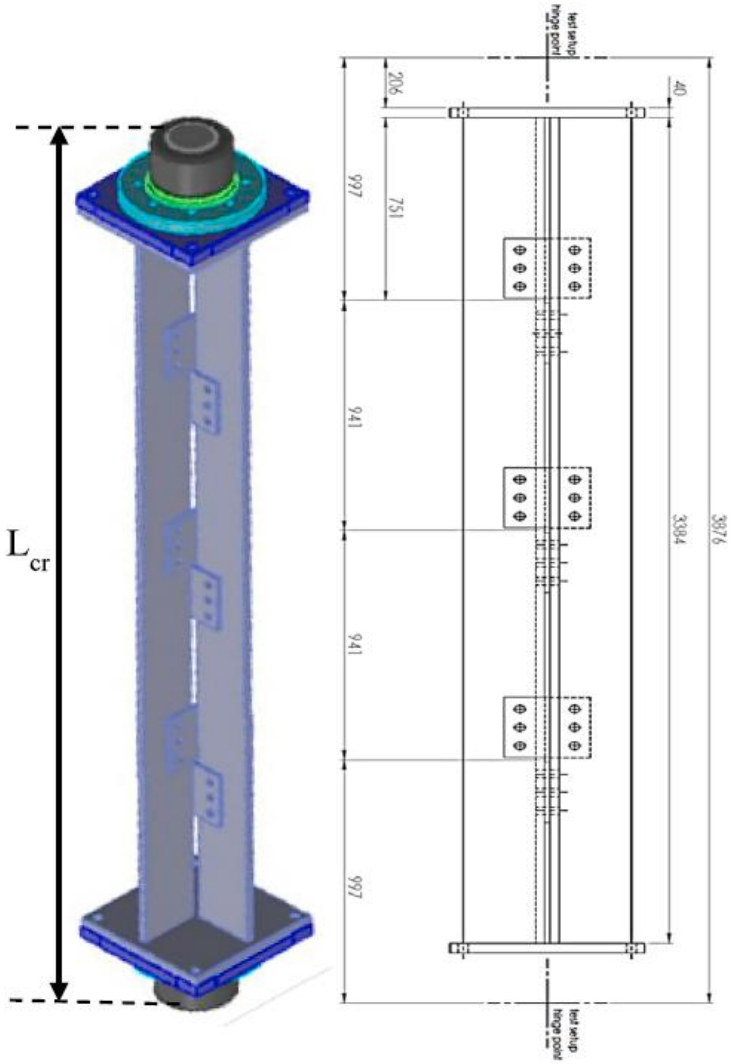

Fig. 14. Buckling length of the tested specimen.

3.2.2. TEST SET-UP AND INSTRUMENTATION

3.2.2.1. Test set-up. The buckling test has been carried out in the OCAS Tubular Testing System (TTS). This test rig has a capacity of 1580 kN in both tension and compression while the maximum length

Published in : Structures (2023), vol. 58, 105274
DOI: 10.1016/j.istruc.2023.105274
Status : Postprint (Author's version)

capacity in between the split couplings is 3800 mm. The system was installed in an explosion-resistant test pit which allows for safe operation given the high loads that were planned to be applied. **Fig. 13** illustrates the buckling specimen installed in the test rig. To attach the specimen to the test rig, two swivel joints were used at its extremities. Being so, the point of rotation was laying outside the specimen (see **Fig. 14**), which extends the buckling length of the test sample to L_{cr} = 3878 mm. The swivel joints (spherical plain bearings) basically allow the specimen to freely rotate around its principal axes. But in reality, for such a test, the low but unavoidable frictional forces are seen sufficient to restrain the specimen from twisting at its supports.

3.2.2.2. Instrumentation. Five displacement transducers were installed on the test specimen as shown in **Fig. 15**; one for the axial deformation (indicated as "Total Displacement" in **Fig. 15**) and four for the lateral displacements of the mid-section (indicated as "Displacement 1 to 4" in **Fig. 15**). At the mid-section, the transducers have been attached using magnets at the mid-height of the legs of the angle profiles. Displacement 1 and 3 measure horizontal displacement, while Displacement 2 and 4 are measuring the vertical ones; their signs are also indicated in **Fig. 15**.

Furthermore, twelve strain gauges have been installed along the specimen. More precisely, three sets of 4 gauges have been placed at 1/ 4, 1/2 and ¾ of the member's length, as schematized in **Fig. 16**.

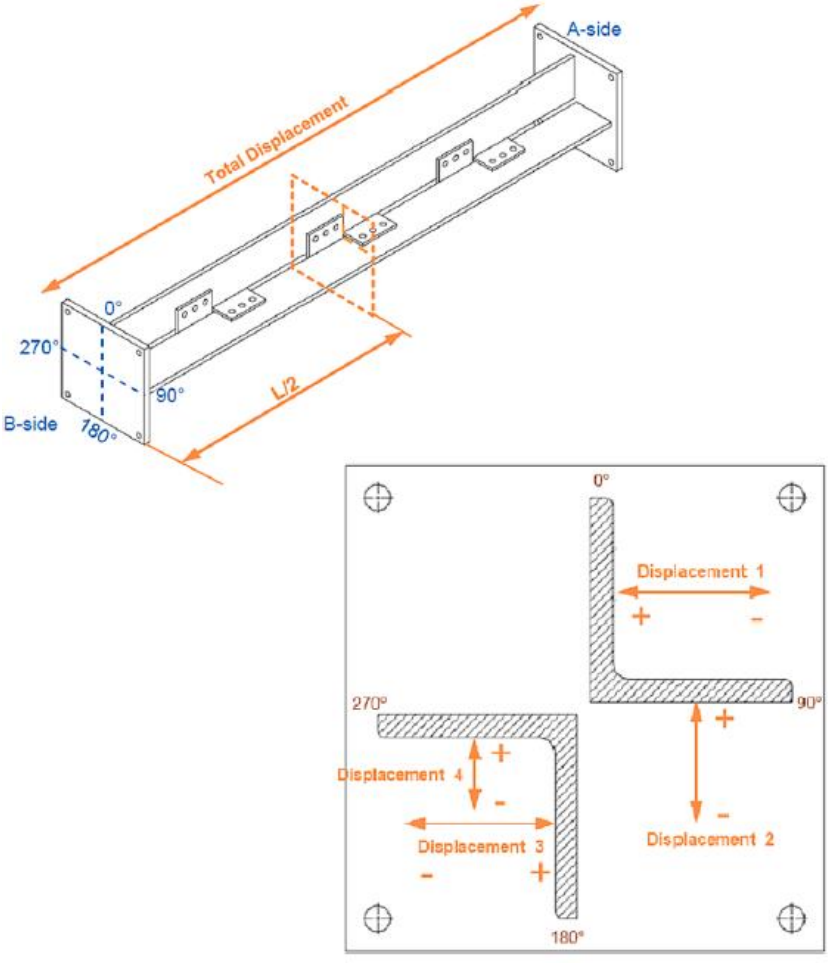

Fig. 15. Location of the displacement sensors.

Published in : Structures (2023), vol. 58, 105274
DOI: 10.1016/j.istruc.2023.105274
Status : Postprint (Author's version)

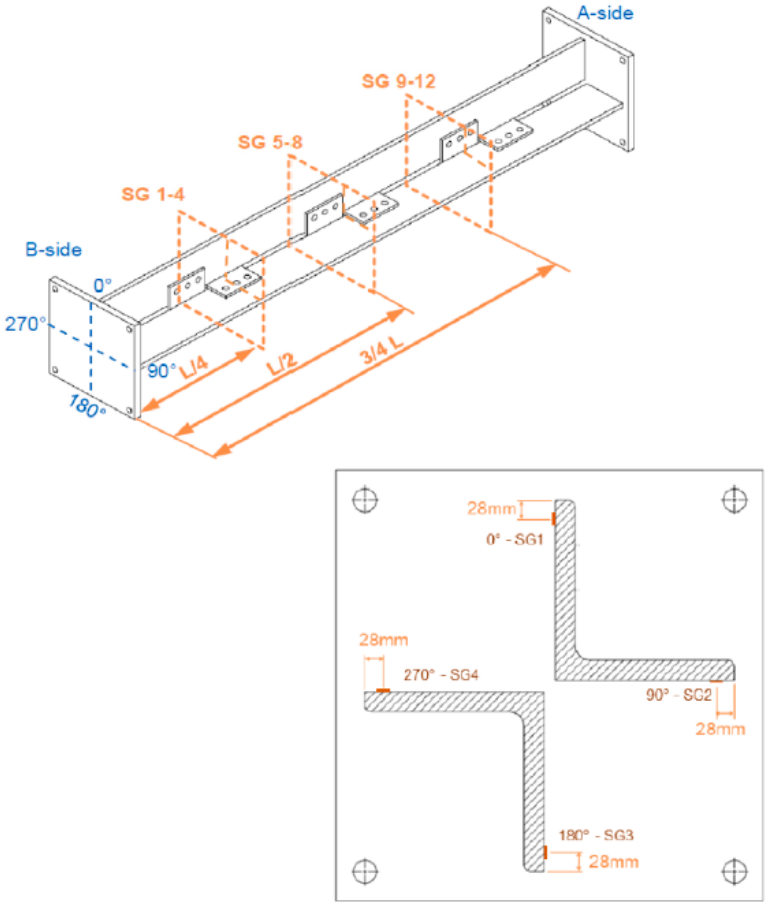

Fig. 16. Location of the strain gauges.

3.2.3. BUCKLING TEST RESULTS

Fig. 17 and **Fig. 18** show the total axial deformation and the lateral displacements of the mid-section respectively versus the compressive load. In addition, the measured strains are reported in **Fig. 19**, **Fig. 20** and **Fig. 21**. After reaching a compressive load of 10,6 MN, yielding initiated. The applied force was further increased up to 10,75 MN, where failure due to buckling occurred. Strain gauges 2 and 11 exhibit values of about 20.000με due to the appearance of plastic deformation, while the strain gauges at the central section (L/2: strain gauges 5 to 8) show values of about 2500με.

Finally, a complex deformation shape has been observed. Both in the horizontal and the vertical plane, the specimen appears to be deformed in an S-shape indicating a global buckling as can be observed in **Fig. 22** but also through the measured lateral displacements, while local buckling of the legs appears at L/4 and 3L/4. Therefore, the member failed due to a combination of both global and local buckling.

3.3. ANALYTICAL CALCULATIONS

Hereafter, the member buckling resistance is evaluated according to the three considered norms described in **section 2**.

Published in : Structures (2023), vol. 58, 105274
DOI: 10.1016/j.istruc.2023.105274
Status : Postprint (Author's version)

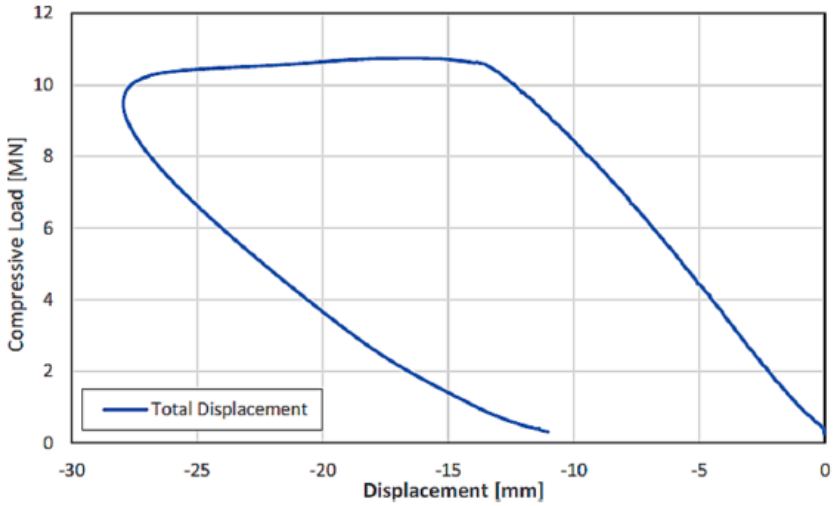

Fig. 17. Axial deformation (total displacement) of the specimen vs the compressive load.

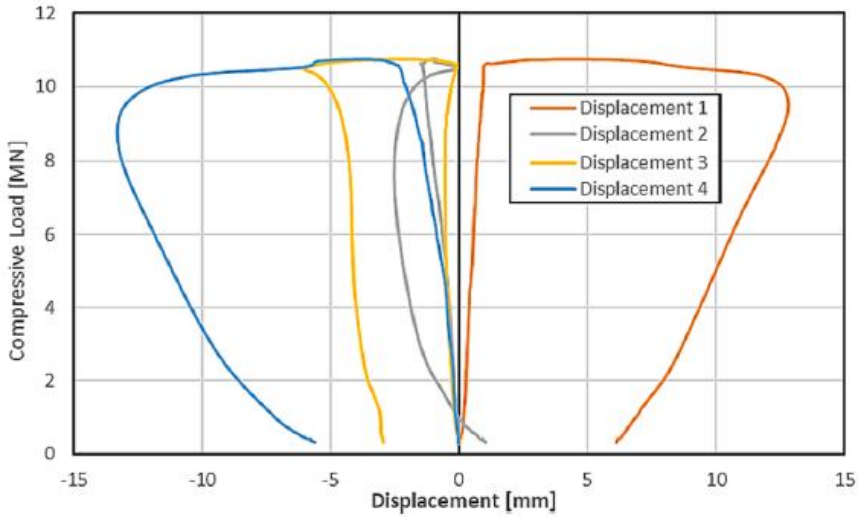

Fig. 18. Lateral displacements of the mid-section vs the compressive load.

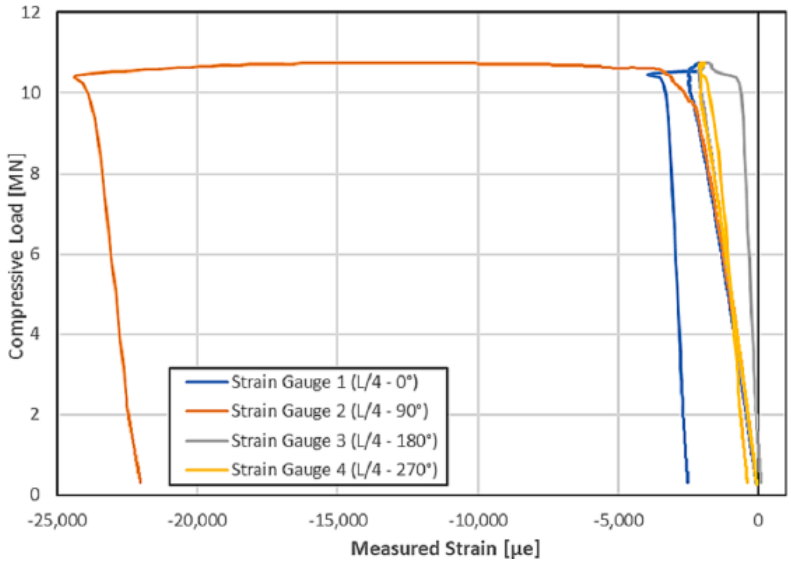

Fig. 19. Measured strain at L/4 vs the compressive load.

Published in : Structures (2023), vol. 58, 105274
DOI: 10.1016/j.istruc.2023.105274
Status : Postprint (Author's version)

3.3.1. CLASSIFICATION OF THE PROFILE

The cross-section may be characterised by the following aspect ratios, depending on the referred normative document:

(i) h/t = 250/28 = 8,98
(ii) (h-2 t)/t = (250-2·28)/28 = 6,93

Table 4 summarizes the class of the L250x250x28 profile according to EN 50341, EN 1993-3-1 and prEN 1993-3 for three different yield strengths.

As already explained in **section 2.1.1**, it is quite impossible to find a reasonable interpretation of EN 1993-1-1, EN 1933-1-5 and EN 50341 for the classification and the evaluation of the effective area. However, if a strict application of the existing provisions is followed, then **Eq. (3)** gives (for $\bar{b}$ = h and k_σ = 0,43) a maximum plate slenderness equal to 0,671 which corresponds to f_y = 460 MPa. For $\bar{\lambda}_p \leq$ 748, ρ is equal to 1,0, which clearly highlights the inconsistency between the codes where a class 4 profile has finally a non-reduced area.

3.3.2. BUCKLING RESISTANCE OF THE MEMBER

For the calculations of the buckling resistance, the critical length has been taken equal to L_{cr} = 3878 mm, which corresponds to the actual one during the test. It should also be mentioned that for the studied member, the distance between the batten pairs of batten plates is much shorter than $50i_{min}$ while the free distance is nearly the same as the connected one. Therefore, according to EN1993-1-1 the member can be considered as an integral member, and thus the shear flexibility or its connections may be neglected (i.e. $S_v = \frac{24EI_{v,ch}}{a^2}$). **Table 5** summarizes the analytical calculations and the evaluation of the code resistances. Checks that are not required by the considered norm are indicated through dashed lines in the table.

Amongst the three standards, EN 1993-3-1 looks to be the most conservative one, while EN 50341 predicts quite well the experimental resistance; prEN 1993-3 gives intermediate values. However, according to Section 7.3.9 of EN50341, the experimental result should be 5 % higher than the resistance value got through the application of Annex J.4 rules. And if this condition is not satisfied, further calculations have to be achieved so as to derive a new f_y value to be used in Annex J.4. On the contrary, prEN 1993-3 which has been scientifically and experimentally validated for high strength steels within the ANGELHY project [11], is always on the safe side but not too conservative, especially if we count on f_y = 460 MPa as it is allowed in some countries.

3.4. NUMERICAL SIMULATIONS

The objective of the numerical simulations is to recreate the conditions of the buckling test taking into account the actual measured imperfections and material properties and to compare the results of the numerical simulation with those obtained in laboratory through a buckling test.

Published in : Structures (2023), vol. 58, 105274
DOI: 10.1016/j.istruc.2023.105274
Status : Postprint (Author's version)

3.4.1. MODELLING OF THE MEMBER

3.4.1.1. Geometry and boundary conditions. The numerical simulations were carried out with the ANSYS software [24], using the solid element "Solid 186" from its element library (see Fig. 23). This is a 20-node element (8 nodes at the vertices and 12 nodes in the middle) with three degrees of freedom each (displacements along the ×, y and z axis).

In order to represent the real stiffness of the built-up section, several contact regions were defined, as they are shown in the **Fig. 24**(a). For the contact between the nut and the angle and the contact between the packing plates and the angle, a friction coefficient equal to 0,2 has been applied; this value is considered as a lower bound. Nonetheless, as the bolts are not preloaded the value of the friction coefficient has been shown to have very low influence [17]. In addition, a clearance of 2 mm in bolt holes has been modelled, in order to account for the sliding before contact.

The boundary conditions applied in the numerical model are represented schematically in **Fig. 24**(b). It should be noted that the rotations about the axis Y (denoted w_x) and Z (denoted v_x) are free, while the torsional rotations φ (rotations about the longitudinal axis) are restrained. In addition, the load is introduced by an imposed axial displacement u applied to one end of the member.

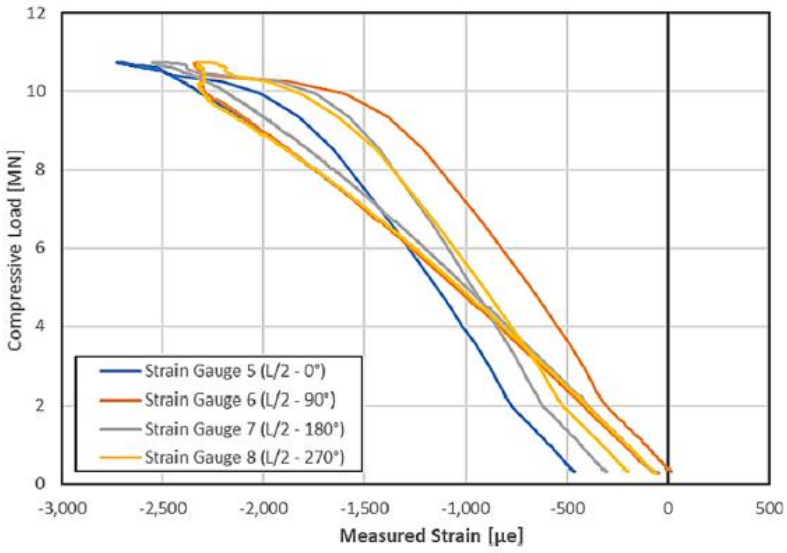

Fig. 20. Measured strain at L/2 vs the compressive load.

Published in : Structures (2023), vol. 58, 105274
DOI: 10.1016/j.istruc.2023.105274
Status : Postprint (Author's version)

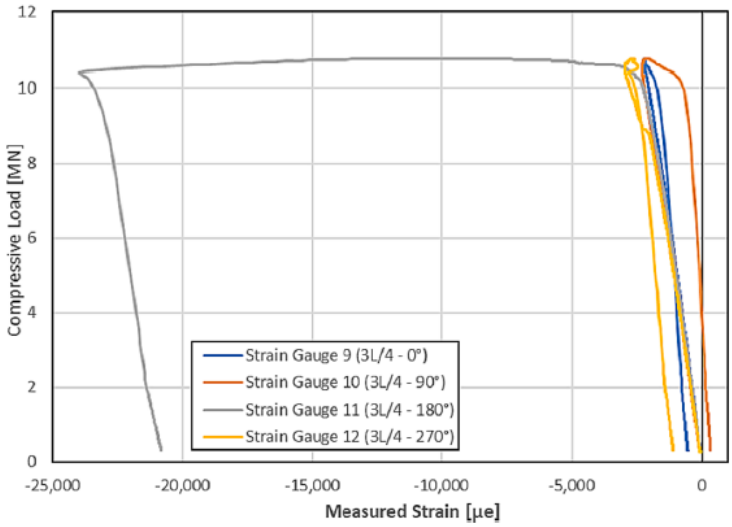

Fig. 21. Measured strain at 3L/4 vs the compressive load.

Table 4
Classification of the angle L250x250x28.

f_y [MPa]	EN 50341 $h/t \leq 11{,}5\varepsilon$	EN 1993–3-1 $(h\text{-}2\ t)/t \leq 11{,}5\varepsilon$	prEN 1993–3 $(h\text{-}2\ t)/t \leq 14{,}0\varepsilon$
440 ($\varepsilon = 0{,}731$)	Class 4	Class 3	Class 3
445 ($\varepsilon = 0{,}727$)	Class 4	Class 3	Class 3
460 ($\varepsilon = 0{,}714$)	Class 4	Class 3	Class 3

3.4.1.2. Geometrical imperfections. The following geometric imperfections have been taken into account in the numerical model:

- The straightness imperfection of the centroid of the section. It has been assumed that this straightness imperfection coincides with the measures taken at mid height of the legs. This imperfection triggers the flexural buckling.
- The straightness imperfection of the outstand flanges of the angles: a linear interpolation has been carried out with the measures taken at mid height and at quarter height from the free end of each angle flange. This imperfection tends to induce local buckling of the flanges.
- The endplate eccentricity by making an offset of the application were carried out with the ANSYS software [24], using the solid element point of the force.

It should be noted that the values of these imperfections are in accordance with the measured ones, as they have been described in **section 3.2.1.1**. However, as the measurements have been taken discontinuously, a linear interpolation has been applied between each measurement (in the longitudinal direction and over the leg width).

Published in : Structures (2023), vol. 58, 105274
DOI: 10.1016/j.istruc.2023.105274
Status : Postprint (Author's version)

Fig. 22. Final deformation of the specimen.

Table 5
Analytically obtained resistances.

	EN 50341, Annex J.4			EN 1993-3-1			prEN 1993-3, Annex F		
f_y [MPa]	440	460	445	440	460	445	440	460	445
Flexural buckling check about v-v axis:									
$\overline{\lambda}_{eff,F} = \frac{L_{cr}/i_{min}}{\pi\sqrt{\frac{E}{f_y}}}$[-]	0,592	0,605	0,592	0,592	0,605	0,592	0,592	0,605	0,592
Flexural buckling check about u-u axis:									
$N_{cr,u} = EI_{u,GS}\left(\frac{\pi}{L_{cr}}\right)^2$ [MN]	—	—	—	—	—	—	55,93	55,93	56,69
$S_v = \frac{24EI_{v,ch}}{a^2}$[MN]	—	—	—	—	—	—	178,78	178,78	181,18
$N_{cr,Sv} = \frac{1}{\frac{1}{N_{cr,u}}+\frac{1}{S_v}}$[MN]	—	—	—	—	—	—	42,61	42,61	43,17
$\overline{\lambda}_{Sv} = \sqrt{\frac{N_{Rk}}{N_{cr,Sv}}}$[-]	—	—	—	—	—	—	0,524	0,536	0,524
Torsional buckling check:									
$N_{cr,T} = \frac{1}{r_0^2}\left(GI_T+\frac{\pi^2 EI_w}{L_{cr,T}^2}\right)$ [MN]	23,08	23,08	23,38	23,08	23,08	23,38	—	—	—
$\overline{\lambda}_{eff,T} = \sqrt{\frac{2Af_y}{N_{cr,T}}}$[-]	0,712	0,728	0,711	0,712	0,728	0,711	—	—	—
Compound member check:									
$\overline{\lambda}_u = \sqrt{\left(\frac{L}{i_{max}}\right)^2+\left(\frac{a}{i_{min,ch}}\right)^2\frac{m}{2}}$[-]	36,89	36,89	36,89	—	—	—	—	—	—
$\overline{\lambda}_{eff,u} = \frac{\lambda_u}{\pi\sqrt{\frac{E}{f_y}}}$[-]	0,537	0,550	0,537	—	—	—	—	—	—
Buckling resistance									
$\overline{\lambda}_{eff}$[-]	0,712	0,728	0,711	0,712	0,728	0,711	0,592	0,605	0,592
α [-]	0,13	0,13	0,13	0,34	0,34	0,34	0,34	0,34	0,34
χ [-]	0,892	0,885	0,892	0,777	0,768	0,777	0,841	0,834	0,841
$N_{b,Rd} = \frac{\chi Af_y}{\gamma_{M1}}$[MN]	10,44	10,83	10,56	9,09	9,39	9,20	9,84	10,21	9,96
Comparison with the experimental result (N_{exp} = 10,75 MN)									
$n = N_{exp} / N_{b,Rd}$ [-]	1,03	0,99	1,02	1,18	1,14	1,17	1,09	1,05	1,08

Published in : Structures (2023), vol. 58, 105274
DOI: 10.1016/j.istruc.2023.105274
Status : Postprint (Author's version)

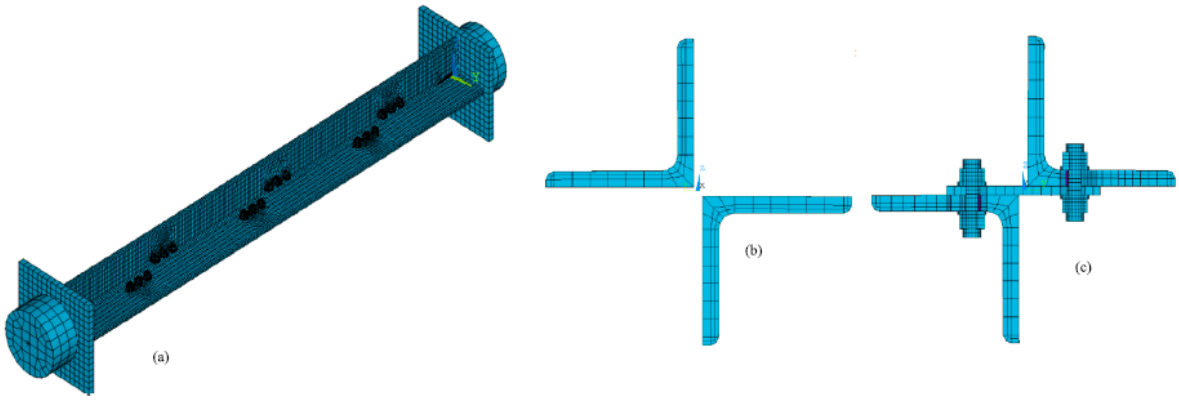

Fig. 23. (a) Overview of the numerical model, (b) built-up section in common area and (c) built-up section in connection area.

3.4.1.3. Material mechanical properties. Residual stress has been implemented in the numerical model in accordance with those illustrated in **Fig. 11**; a linear interpolation between two points of measurement (i.e. interior / exterior) has been carried out. Moreover, a simplified multilinear material law with the values of f_y and f_u measured in the laboratory has been retained in accordance with **Fig. 25**. The Young's modulus E was taken equal to the measured one. For the batten plates, the same material law has been applied. Nevertheless, due to a low level of load through the packing plates, the result of the numerical model is not influenced by the plastic properties.

The bolts are assumed to be class 8.8. However, as for the packing plates, the material law applied to the bolts does not influence the stiffness of the built-up member.

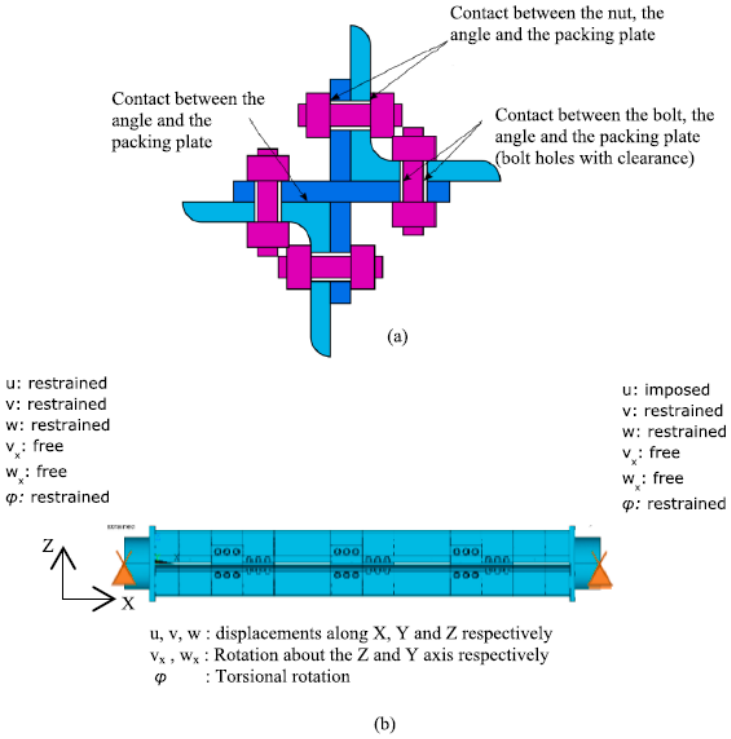

Fig. 24. (a) Contact regions in the built-up section and (b) schematic representation of the support conditions of the numerical model.

Published in : Structures (2023), vol. 58, 105274
DOI: 10.1016/j.istruc.2023.105274
Status : Postprint (Author's version)

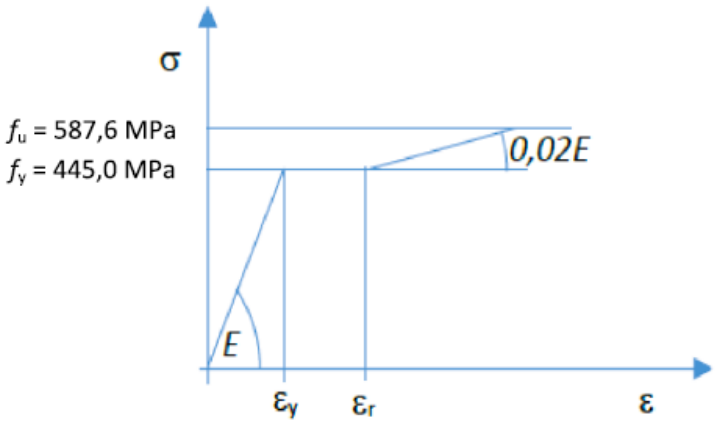

Fig. 25. Material law in accordance with references [5,37].

3.4.2. NUMERICAL RESULTS OF THE TESTED MEMBER

Firstly, in order to determine the eigenmode of elastic buckling an elastic instability analysis has been carried out with the Ansys software (LBA analysis: Linear Bifurcation Analysis). It should be noted that the LBA calculation cannot consider non-linear effects as contact. Thus, the contact status of the different regions is based on their initial situation, i.e. regions where contact was initially detected (contact is close) are calculated as in contact whereas regions where no contact is detected initially (contact is open) are calculated as without contact. The results are summarized in **Table 6**, where several elastic buckling modes may be identified. Buckling modes characterized by quasi rigid body rotation about one point (close to the effective centroid of the built-up member) are referred to as elastic torsional buckling mode. Additionally, one may identify elastic buckling modes characterized by displacements that are more pronounced in one angle section than in the second one. These modes are referred to as flexural torsional buckling mode of an individual member. This mode may potentially also be characterized as local buckling occurring in the built-up member. A clear local buckling mode of an individual angle, as one might observe more easily in case of high width to thickness ratios, does not occur in the first five elastic buckling modes.

In order to determine the failure load of the member, a full non-linear analysis has been performed by imposing a successive increase of the longitudinal displacement on one of the supports. The analysis ends when the axial force induced in the member at a step *i* is less than the axial force obtained by imposing force at the step $i - 1$, which physically results in the fall of the stiffness of the beam. In order to represent the post buckling behaviour, the calculation is continued up to a reaction force that is less than approximately 95 % of the maximum load. In this case, the failure load corresponds to the maximum value of the normal force.

The comparison between the curves of the load versus the axial shortening of the specimen as obtained in laboratory and by the numerical analysis is shown in **Fig. 26**. It can be noted that the experimental ultimate axial force (10,75 MN) is quite similar with the numerical one (10,28 MN). However, the stiffness and the value of the displacement at which the ultimate axial force is reached differ.

Published in : Structures (2023), vol. 58, 105274
DOI: 10.1016/j.istruc.2023.105274
Status : Postprint (Author's version)

In order to further analyse the difference between laboratory test and numerical simulation, it is interesting to study the axial strains. In **Fig. 26**, we can observe that the ultimate axial force is reached after a transition from the elastic to plastic behaviour. Subsequently, the strain at which the ultimate axial force is reached should be close to the elastic one $\varepsilon_y = f_y/E$ = 445/212800 = 0,21 %. The value of this strain may also be determined approximatively based on the axial shortening of the member (the axial displacement) by:

- δ/L = 7,7/3384 = 0,23 % for the numerical simulation;
- δ/L = 13/3384 = 0,38 % for the laboratory test.

The value of the strain at which the ultimate axial forced is reached seems consistent with **Fig. 19** to the **Fig. 21**. A final comparison is given in **Fig. 27** showing the load–displacement curves obtained from the laboratory test and the numerical simulation as well as the evolution of axial displacements back calculated from the measured mean strain values at the three locations along the member (i.e. axial displacements 1, 2 and 3 are based on mean axial strains at 1/4L, 1/2L and 3/4L respectively). The axial displacement "u_x" is obtained by:

$$u_x = L \cdot \overline{\varepsilon}_x \qquad (8)$$

where L is the member length between end plates (3384 mm) and $\overline{\varepsilon}_x$ is the mean value of axial strains (obtained from the four measurements in one section) at L/4, L/2 and 3L/4.). As expected, the measured strains at the three positions are almost the same and equal to 0,23 as the member is subjected to compression only. Therefore, the obtained estimation of the evolution of axial displacements with the applied loads seems to confirm the initial stiffness of the numerical model, while the total longitudinal displacement measurement during the test looks to be inaccurate and inappropriate due to the bending deformations developed in the specimen during testing.

The displacements of the numerical simulations are shown in **Figs. 28–30**. It can be noted that the displacements indicate a global flexural buckling, with the presence of a slight local buckling of the legs (outstand flange). Indeed, one may note that the local displacements along a leg are low compared to the mid-span displacements of the member. However, the mid-span displacements themselves remain low at failure. As the member is rather stocky, flexural buckling is not very significant (relative slenderness is low and strength reduction due to instability is low as well).

Fig. 31 shows the comparison of the load versus the lateral displacements obtained through the laboratory test and the numerical simulations. The notations and signs of the displacements are according to **Fig. 15**. It can be seen that both numerical and experimental specimens are moving in the same vertical direction but not in the same horizontal one. Furthermore, the numerical and experimental stiffness of the specimen is quite close, especially in the vertical plane (displacements 2 and 4).

In conclusion, the numerical model gave a value of the ultimate resistance to the axial force equal to 10,28 MN which is about 4 % lower than the laboratory test result. Furthermore, in both cases, the failure mode of the built-up member seems to be a combination of the global buckling of the member with a contribution of local buckling of the flanges. Although in the numerical model local buckling is

Published in : Structures (2023), vol. 58, 105274
DOI: 10.1016/j.istruc.2023.105274
Status : Postprint (Author's version)

less pronounced, it can be seen by the deformed shape of the cross-section in **Fig. 29**, while the following points may explain the differences with the buckling test:

- The straightness measurements have been carried out at the mid and quarter height, which makes it harder to differentiate the straightness imperfection of the centroid (member imperfection) and the straight imperfection of the flanges (plated imperfection). In the numerical simulation, a simplified assumption on local imperfection is applied.
- The residual stress measurements have been carried out for one angle section. It could be supposed that the initial stress in the section where the failure has occurred, was slightly different and that the distribution of residual stresses was influenced by the presence of the holes.

Published in : Structures (2023), vol. 58, 105274
DOI: 10.1016/j.istruc.2023.105274
Status : Postprint (Author's version)

Table 6
Results of LBA.

Elastic critical buckling mode number	Global view of mode	Cross section view of mode	Elastic buckling mode	Elastic critical load [MN]
1	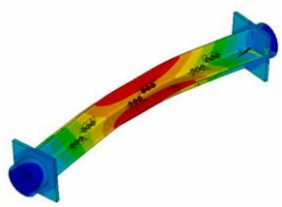	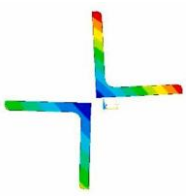	Flexural-torsional buckling of the individual angles	31,02
2	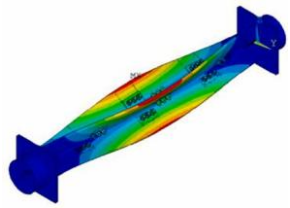	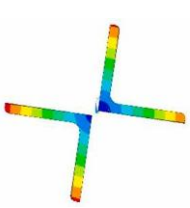	Torsional buckling of the built-up member	31,81
3	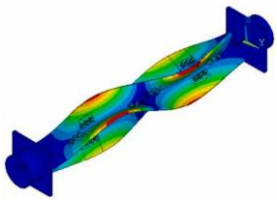	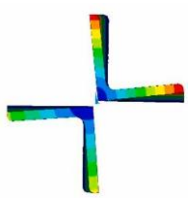	Torsional buckling of the built-up member	36,50
4	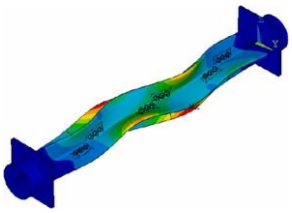	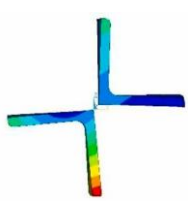	Torsional flexural buckling of the individual angles / Local buckling in the built-up member	41,07
5	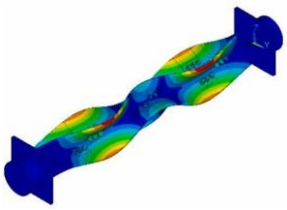	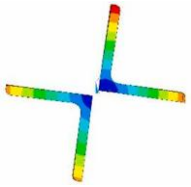	Torsional buckling of the built-up member	42,72

Published in : Structures (2023), vol. 58, 105274
DOI: 10.1016/j.istruc.2023.105274
Status : Postprint (Author's version)

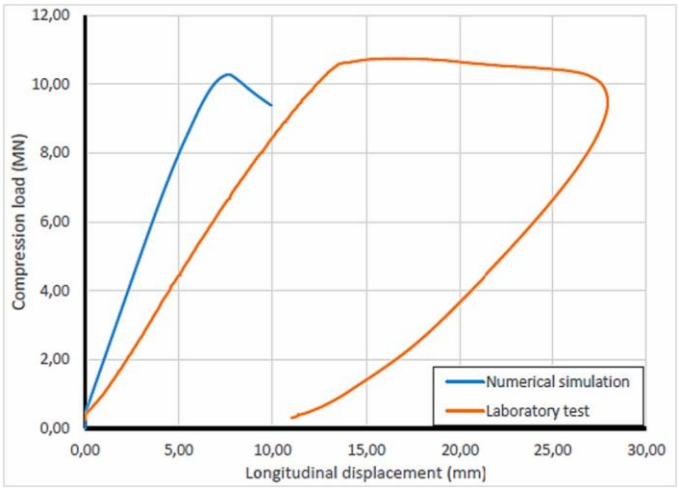

Fig. 26. Load vs axial displacement curve of both numerical simulation and experimental test.

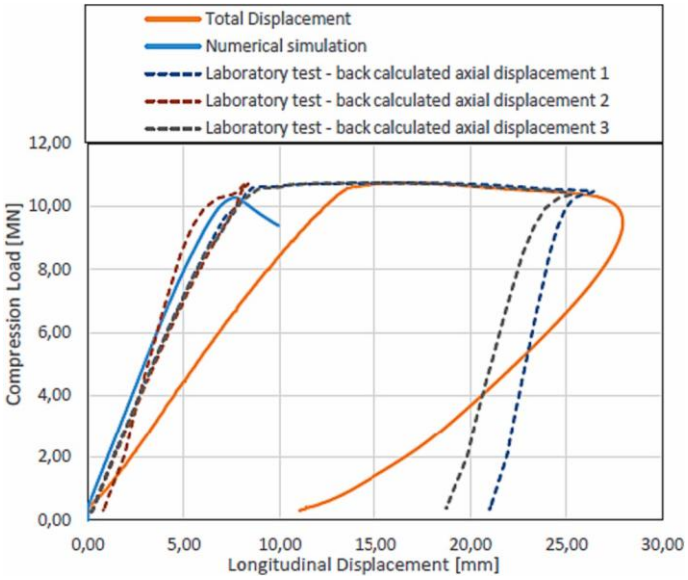

Fig. 27. Load displacement curves with back calculated axial displacements.

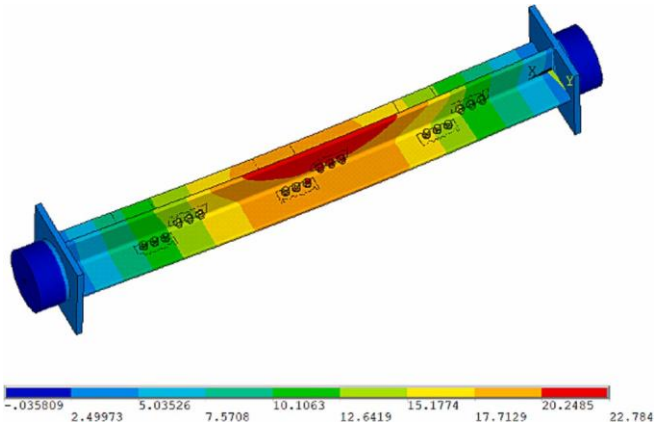

Fig. 28. Transversal displacement along the axis y-y at the last step (mm).

Published in : Structures (2023), vol. 58, 105274
DOI: 10.1016/j.istruc.2023.105274
Status : Postprint (Author's version)

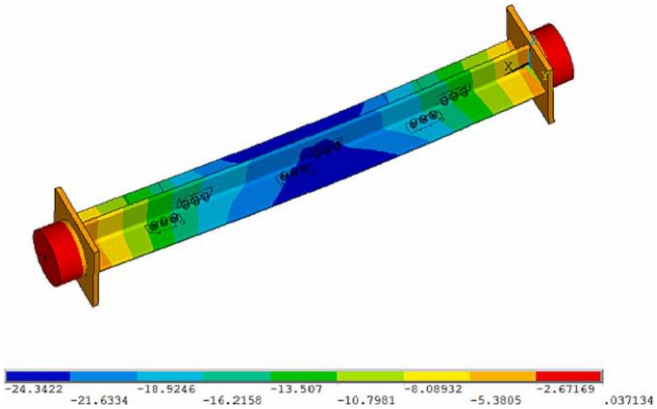

Fig. 29. Transversal displacement along the axis z-z at the last step (mm).

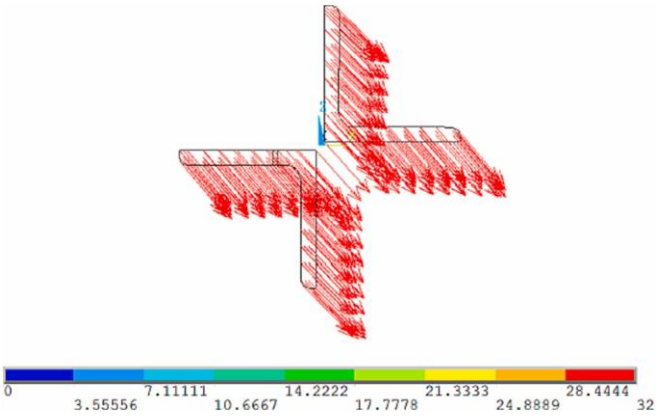

Fig. 30. Displacement vectors of the section at mid-span at the last step (mm).

3.4.3. FURTHER NUMERICAL INVESTIGATIONS

In order to study further the appearance of local buckling during the laboratory test, a second analysis has been performed. In this one, the same input data as for the previous study have been used except the thickness of the upper angle section that is reduced to 25,3 mm (-8% compared to the measured value of 27,3 mm); the thickness of the lower angle sections remains the same (27,3 mm). This very high reduction is probably not realistic but it is assumed for this sensitivity analysis.

First, the elastic buckling modes have again been calculated; the first eigenmode ($N_{cr,1}$ = 27,84 MN) appears to correspond to a flexural–torsional buckling of the built-up member while the second one ($N_{cr,2}$ = 30,15 MN) was a flexural–torsional buckling of the individual angles.

The results of the GMNIA numerical simulations in terms of failure mode and lateral displacement at mid span are provided in **Fig. 32** and **Fig. 33** respectively. The displacement vectors at the last calculation step are shown in **Fig. 34**. The ultimate load for this simulation is equal to $N_{ult,2}$ = 10,29 MN, which is almost identical with the first simulation while in this case local buckling failure of the thinner legs is more pronounced accompanied also by a flexural buckling. The numerical simulation shows again a good agreement with the laboratory test in terms of ultimate load and load displacement paths. Considering the results of the reference simulation presented in **section 3.4.2** and the results of this sensitivity analysis, it might be concluded that the influence of a big reduction of the leg's thickness of one angle to its ultimate resistance is negligible, while the failure mode is strongly

Published in : Structures (2023), vol. 58, 105274
DOI: 10.1016/j.istruc.2023.105274
Status : Postprint (Author's version)

affected. Being so, the failure mode of the experimental test can be easily explained, knowing that a possible local reduction of the thickness (or any other relevant other parameter) of one angle could immediately favour the appearance of local buckling in the specimen but without affecting its ultimate resistance.

Globally, one may conclude that the numerical simulation is very close to the result of the single laboratory test that has been carried out. It may also be noted that the design of the built-up member could be optimized by the following means:

- at each packing plate, 2 bolts instead of 3 would most likely be sufficient to ensure a level of connection almost identical to that obtained by 3 bolts. The central bolt could therefore be removed.
- the distance between the packing plates could be increased. Indeed, a distance of approximately $15i_{min}$ has a small effect on the resistance of the built-up member (in the context of §6.4.4(1) of EN 1993-1-1, the effect of the connection on the resistance may be neglected if the distance is less than $70i_{min}$ for built-up member with batten plates). Moreover, in cases where the failure mode corresponds to a local buckling of the flanges, the distance between the connections has practically no influence on the resistance of the built-up member.

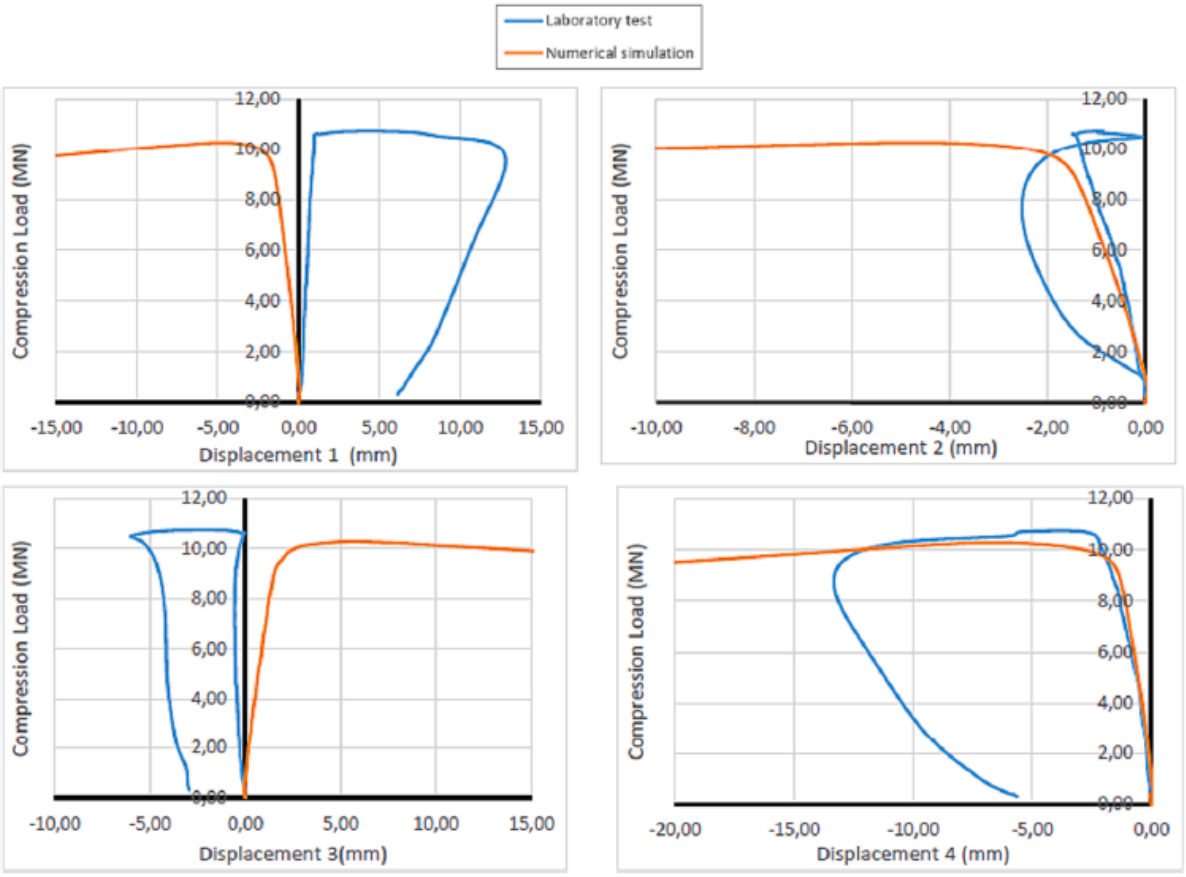

Fig. 31. Comparison of the mid-span displacements between numerical simulation and laboratory test.

Published in : Structures (2023), vol. 58, 105274
DOI: 10.1016/j.istruc.2023.105274
Status : Postprint (Author's version)

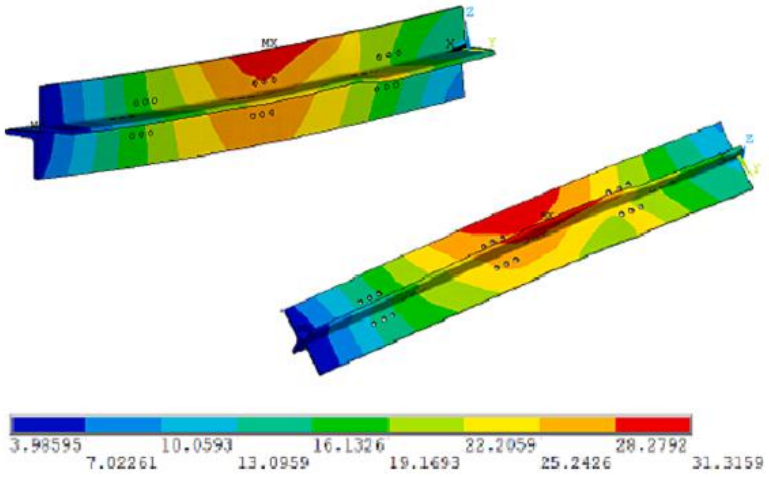

Fig. 32. Displacement vector sum and deformed shape (2 views) of the member at the end of the analysis.

4. Carrying capacity of the SB L300x300x35 S460 member

As explained in the introduction, the bearing capacity of a star- battened member made of two S460 L300x300x35 angles with a member length of 4486 mm needs to be evaluated for its used in a specific transmission tower of 240 m high. **Table 7** summarises the buckling design resistances obtained by the different considered standards.

A full non-linear finite element model with volume elements has been also performed and the numerically determined resistance equals 16,62 MN; the correspondence between prEN1993-3 is quite good with a difference, on the safe side, of 7,8%. The estimation provided by EN 50341 is also precise but remains questionable for the reasons explained in **section 2**. It can be therefore concluded that the resistance of the SB L300x300x35 S460 member evaluated with prEN 1993-3 allows to satisfy the initial request of about 15,0 MN in terms of expected level of resistance, even, as it is the case in Belgium, the use of EN 10025 is recommended (resistance of 14,75 MN).

Published in : Structures (2023), vol. 58, 105274
DOI: 10.1016/j.istruc.2023.105274
Status : Postprint (Author's version)

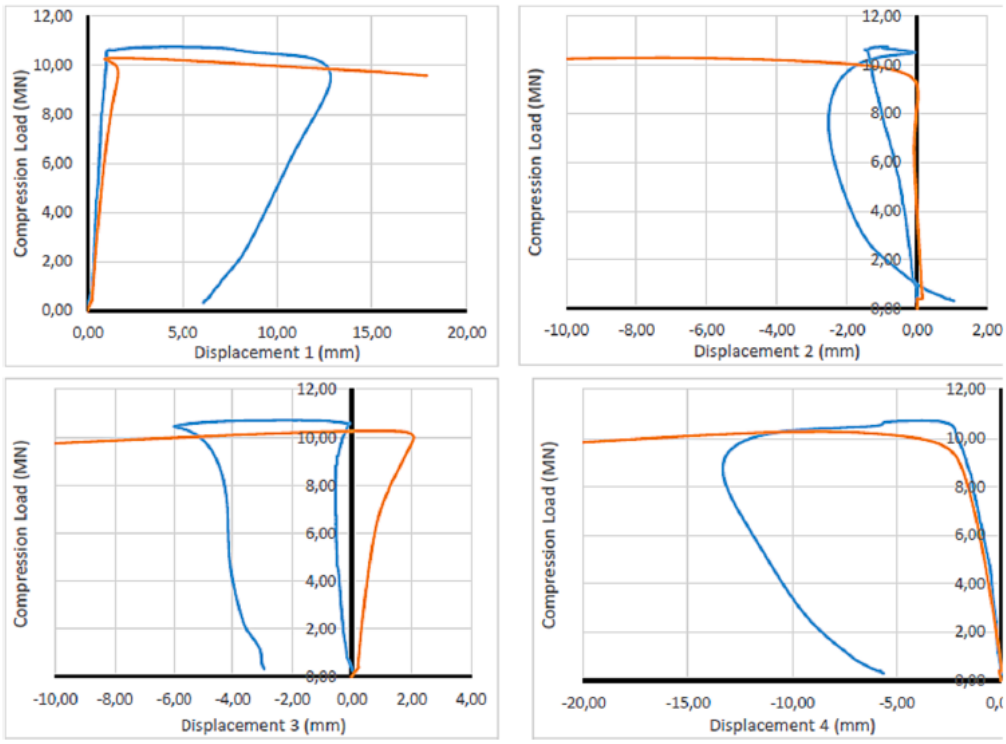

Fig. 33. Comparison of the mid-span displacements between numerical simulation 2 and laboratory test.

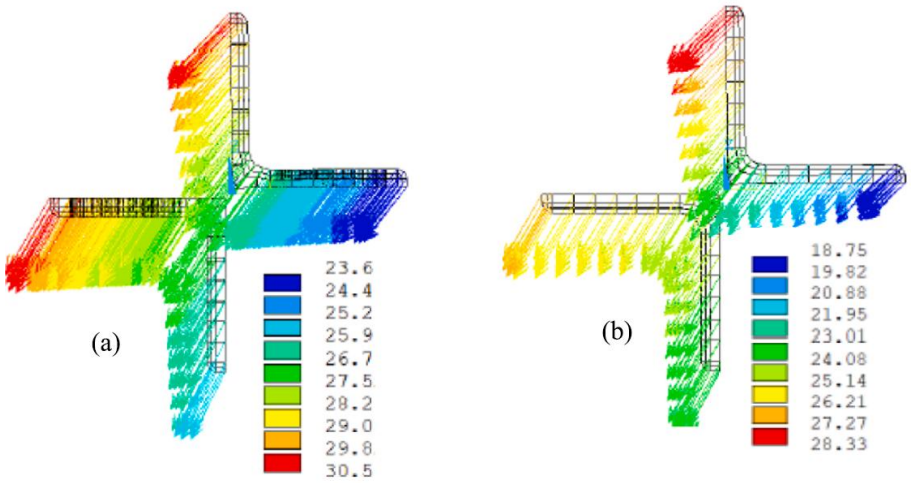

Fig. 34. Displacement vectors (a) at mid-span and (b) at quarter-span at the last calculation step (mm).

Table 7
Summary of the analytically obtained resistances of the SB L300x300x35.

Normative document	Design resistance $N_{b,Rd}$ [MN]	
	$fy = 440$ MPa	$fy = 460$ MPa
EN 50341	15,66	16,27
EN 1993–3-1	13,79	14,27
prEN 1993–3	14,75	15,31

Published in : Structures (2023), vol. 58, 105274
DOI: 10.1016/j.istruc.2023.105274
Status : Postprint (Author's version)

5. Conclusions

The main conclusions of the paper can be summarised as follows:

- Two main European normative documents cover nowadays the design of star-battened members in compression, namely: EN 50341:2012 and EN 1993-3-1:2005. Both extensively refer to EN 1993-1-1:2005 and EN 1993-1-5:2006. Through a careful analysis of these documents, some lacks, contradictions and inconsistencies have been revealed, in particular – but not exclusively – for their application to S460. On the contrary, in a recent European project entitled ANGELHY, an extensive analytical, numerical and experimental study has been performed in which a particular attention has been paid to S460. As a result, a full set of formulae for pin-ended members has been proposed and has been recently implemented in the new forthcoming version of EN 1993-3-1:2005, named prEN 1993-3:2021; however without accounting for the effects of the restraints at the extremities due to the connections.
- A star-battened member has been considered as a case study and its resistance has been evaluated analytically, experimentally and numerically. The application of prEN 1993-3:2021 to the studied member has been achieved and the results have been compared with those provided by EN 50341:2012 and EN 1993-3-1:2005. EN 1993- 3-1 looks to be the most conservative, while EN 50341 predicts quite well the experimental resistance; prEN 1993-3 gives intermediate values. It has also been seen that, for the specimen considered in the case study, EN50341 Annex J.4 cannot be applied as the test resistance is not higher than 5 % of the analytical one and so further calculations are required to satisfy this 5 % criterion.
- The estimation provided by EN 50341 is also quite precise but remains questionable as long as EN 50341 has never been validated for S460 steel and as inconsistencies have been identified in the classification system proposed by EN 50341.
- To validate the normative approaches, a buckling test has been performed. Its ultimate experimental resistance was equal to 10,75 MN and the members fails due to a combination of global member buckling and local buckling of the legs of the angle profiles.
- A full non-linear finite element model with volume elements has been analysed to simulate the response of the member in compression until failure. The numerical model has given a value of the ultimate resistance to the axial force equal to 10,28 MN which is about 4 % lower than the laboratory test result. However, in both cases, the failure mode of the built-up member seems to be a combination of the global buckling of the member with a contribution of local buckling of the flanges.
- A sensitivity analysis has been performed to check the influence of the thickness of the angle profiles to the members response. It has been seen that a reduction of the thickness of one of the angles constituting the profile has no influence on the failure load, but may affects the failure mode as local buckling is more pronounced.
- Finally, an adequate level of resistance of the SB L300x300x35 S460 member with an overall length of 4486 mm for its use in 240 m tower has been reached using prEN 1993-3, even in combination with EN 10025, as the obtained design resistance is of the order of the required one, i.e. about 15,0 MN.

Published in : Structures (2023), vol. 58, 105274
DOI: 10.1016/j.istruc.2023.105274
Status : Postprint (Author's version)

Declaration of Competing Interest

The authors declare that they have no known competing financial interests or personal relationships that could have appeared to influence the work reported in this paper.

References

[1] Sperle J-O, Halberg L. Environmental advantages of using high strength steel. In: The 2nd international conference on clean technologies in the steel industry, Budapest Hungary; 2011. p. 75–85.
[2] Saufnay L, Demonceau J-F. Economic and environmental assessment of high- strength steel grades. Ernst & Sohn, ce/papers, Special Issue: EUROSTEEL 2023;6 (3–4):527–32.
[3] EN 1993-3-1: Design of steel structures - Part 3-1: Towers, musts and chimneys. Tower and musts, Brussels, Comité Européen de Normalisation (CEN), 2005.
[4] EN 1993-1-1: Design of steel structures - Part 1-1: General rules and rules for buildings, Brussels, Comité Européen de Normalisation (CEN), 2005.
[5] EN 1993-1-5: Design of steel structures - Part 1-5: Plate structural elements, Brussels, Comité 000.Europeen de Normalisation (CEN), 2006.
[6] EN 1993-1-8: Design of steel structures - Part 1-8: Design of joints, Brussels, Comité Européen de Normalisation (CEN), 2005.
[7] EN 50341-1: Overhead electrical lines exceeding AC 1 kV - Part 1: General requirements - Common specifications, 2012.
[8] Vayas I, Jaspart JP, Bureau A, Tibolt M, Reygner S, Papavasiliou M, Telecommunication and transmission lattice towers from angle sections – the ANGELHY project, doi: 10.1002/cepa, Ernst & Sohn, ce/papers, Special Issue: EUROSTEEL 2021 Sheffield — Steel's coming home, Vol. 4, Issue 2 – 4, 2021. pp. 210-217.
[9] EN 10025-2: Hot rolled products of structural steels - Part 2: Technical delivery conditions for non-alloy structural steels, Comité Européen de Normalisation (CEN), 2019.
[10] Bezas M-Z. Design of lattice towers from hot-rolled equal leg steel angles. University of Liége & National Technical University of Athens; 2021. PhD thesis.
[11] Innovative solutions for design and strengthening of telecommunications and transmission lattice towers using large angles from high strength steel and hybrid techniques of angles with FRP strips, Grant Agreement number: 753993 — ANGELHY — RFCS-2016/RFCS-2016.
[12] prEN 1993-3: Design of steel structures - Part 3: Towers, musts and chimneys, Brussels, Comité Européen de Normalisation (CEN), 2021.
[13] Schillo N, Feldmann M. Buckling resistance of L-profiles in towers, masts and open line Constructions, Stahlbau 84. Heft 2015;12:946–54.
[14] Bezas MZ, Demonceau JF, Vayas I, Jaspart JP. Classification and cross-section resistance of equal-leg rolled angle profiles. J Constr Steel Res 2021;185:106842. https://doi.org/10.1016/j.jcsr.2021.106842.
[15] Bezas M-Z, Demonceau J-F, Vayas I, Jaspart J-P. Design rules for equal-leg angle members subjected to compression and bending. J Constr Steel Res 2022;189: 107092.
[16] Timo˘senko SP. Theory of Elastic Stability. New York, NY: McGraw-Hill; 1961.
[17] Beyer A, Bureau A, Jaspart J-P. Buckling resistance of compression members with back-to-back connected angle sections. Proc Civil Eng 2021;4(2-4):2132–9.
[18] Saufnay L, Beyer A, Jaspart JP, Demonceau JF. Experimental and numerical investigations on closely spaced built-up members. J Struct Eng 2023;Vol. 149, Issue 4. https://doi.org/10.1061/JSENDH.STENG-11642.
[19] Kayser MG, Sarquis F, de Lima LRO, da Silva AT, Rodrigues MC. Numerical assessment of stainless steel starred angle sections under compression. J Constr Steel Res 2023;210.
[20] Behzani-Sofiani B, Gardner L, Wadee MA. Behavior, finite element modelling and design of cruciform section steel columns. Thin-Walled Struct 2023;182:110124.
[21] Botelho IS, da Silva Vellasco PCG, de Lima LRO, Rodrigues MC, da Silva AT. An assessment of starred rolled stainless steel angle columns. 9th International Conference on Steel and Aluminium Structures. 2019.
[22] Kitipornchai S, Lee HW. Inelastic experiments on angle and tee struts. J Constr Steel Res 1986;6(3):219–36.
[23] Lu C, Ma X, Mills JE. The structural effect of bolted splices on retrofitted transmission tower angle members. J Constr Steel Res 2014;95:263–78.
[24] Ansys® Academic Research Mechanical, Release 18.2.

Published in : Structures (2023), vol. 58, 105274
DOI: 10.1016/j.istruc.2023.105274
Status : Postprint (Author's version)

[25] NBN EN 50341-2-2:2019: Overhead electrical lines exceeding AC 1 kV - Part 2-2: National Normative Aspects (NNA) for Belgium (based on EN50341-1:2012), 2019.
[26] NBN EN 1993-3-1 ANB: 2011: Design of steel structures - Part 3-1: Towers, masts and chimneys. Tower and musts, Belgian National Annex, 2011.
[27] Beyer A, Bureau A, Jaspart J-P, Demonceau J-F, Bezas M-Z. Torsional, flexural and torsional-flexural buckling of angle section members – an analytical approach. International Conference on Modelling and Simulation, ICMS 2021, Poznan Poland. 2021.
[28] Beyer A, Delacourt G, Bureau A. Deliverable 3.4: Development of design rules for closely spaced built-up angle sections. CTICM France: Research Report-ANGELHY project; 2020.
[29] Timoshenko S-P, Gere J-M. Theory of Elastic Stability. 2nd ed. Mc Graw Hill International Book Company; 1963.
[30] Modified slenderness ratio for built-up members, Sato and Uang, Engineering Journal, 2007.
[31] NBN EN 1993-1-1 ANB: Design of steel structures - Part 1-1: General rules and rules for buildings, Brussels, Belgian National Annex, 2018.
[32] Wittenberghe, J. (2022) Buckling Test on Transmission Pole for AM R&D Esch ocas, New steel project report, ArcelorMittal, Belgium.
[33] Bezas MZ, Demonceau JF, Jaspart JP. Measurements of residual stresses and characterisation of material properties, New steel project report. Belgium: Universite de Liege; 2022.
[34] EN ISO 6892 – 1: Metallic materials – Tensile testing – Part 1: Method of test at room temperature, Brussels, Comité Européen de Normalisation (CEN), 2016.
[35] Zhang L, Jaspart JP, (2013) Stability of members in compression made of large hot- rolled and welded angles, Research Report, University of Liège.
[36] ECCS, Manual on stability of steel structures, European Convention for Constructional Steelwork, 1976.
[37] ECCS TC 8 (1984), « Ultimate Limit State Calculation of Sway frames with Rigid Joints", ECCS publication n°33.